

Radio sources in the 2dF Galaxy Redshift Survey – II. Local radio luminosity functions for AGN and star-forming galaxies at 1.4 GHz

Elaine M. Sadler,^{1★} Carole A. Jackson,² Russell D. Cannon,³ Vincent J. McIntyre,⁴ Tara Murphy,¹ Joss Bland-Hawthorn,³ Terry Bridges,³ Shaun Cole,⁵ Matthew Colless,² Chris Collins,⁶ Warrick Couch,⁷ Gavin Dalton,⁸ Roberto De Propris,⁷ Simon P. Driver,⁹ George Efstathiou,¹⁰ Richard S. Ellis,¹¹ Carlos S. Frenk,⁵ Karl Glazebrook,¹² Ofer Lahav,¹⁰ Ian Lewis,³ Stuart Lumsden,¹³ Steve Maddox,¹⁴ Darren Madgwick,¹⁰ Peder Norberg,⁵ John A. Peacock,¹⁵ Bruce A. Peterson,² Will Sutherland⁸ and Keith Taylor¹¹

¹*School of Physics, University of Sydney, NSW 2006, Australia*

²*Research School of Astronomy and Astrophysics, The Australian National University, Weston Creek, ACT 2611, Australia*

³*Anglo-Australian Observatory, PO Box 296, Epping, NSW 2121, Australia*

⁴*Australia Telescope National Facility, CSIRO, PO Box 76, Epping, NSW 2121, Australia*

⁵*Department of Physics, South Road, Durham DH1 3LE*

⁶*Astrophysics Research Institute, Liverpool John Moores University, Twelve Quays House, Birkenhead L14 1LD*

⁷*Department of Astrophysics, University of New South Wales, Sydney, NSW 2052, Australia*

⁸*Department of Physics, Keble Road, Oxford OX1 3RH*

⁹*School of Physics and Astronomy, North Haugh, St Andrews, Fife KY6 9SS*

¹⁰*Institute of Astronomy, University of Cambridge, Madingley Road, Cambridge CB3 0HA*

¹¹*Department of Astronomy, Caltech, Pasadena, CA 91125, USA*

¹²*Department of Physics and Astronomy, Johns Hopkins University, Baltimore, MD 21218-2686, USA*

¹³*Department of Physics, University of Leeds, Woodhouse Lane, Leeds LS2 9JT*

¹⁴*School of Physics and Astronomy, University of Nottingham, Nottingham NG7 2RD*

¹⁵*Institute for Astronomy, University of Edinburgh, Royal Observatory, Blackford Hill, Edinburgh EH9 3HJ*

Accepted 2001 September 4. Received 2001 August 20; in original form 2001 June 14

ABSTRACT

We have cross-matched the 1.4-GHz NRAO VLA Sky Survey (NVSS) with the first 210 fields observed in the 2dF Galaxy Redshift Survey (2dFGRS), covering an effective area of 325 deg^2 (about 20 per cent of the final 2dFGRS area). This yields a set of optical spectra of 912 candidate NVSS counterparts, of which we identify 757 as genuine radio identifications – the largest and most homogeneous set of radio source spectra ever obtained. The 2dFGRS radio sources span the redshift range $z = 0.005$ to 0.438 , and are a mixture of active galaxies (60 per cent) and star-forming galaxies (40 per cent). About 25 per cent of the 2dFGRS radio sources are spatially resolved by NVSS, and the sample includes three giant radio galaxies with projected linear size greater than 1 Mpc. The high quality of the 2dF spectra means we can usually distinguish unambiguously between AGN and star-forming galaxies. We make a new determination of the local radio luminosity function at 1.4 GHz for both active and star-forming galaxies, and derive a local star formation density of $0.022 \pm 0.004 \text{ M}_\odot \text{ yr}^{-1} \text{ Mpc}^{-3}$ ($H_0 = 50 \text{ km s}^{-1} \text{ Mpc}^{-1}$).

Key words: galaxies: active – galaxies: luminosity function, mass function – galaxies: starburst – radio continuum: galaxies.

1 INTRODUCTION

Radio source surveys are ideal tools for studying the distant Universe, since they are unaffected by dust obscuration and detect

large numbers of galaxies over a wide span of cosmic epochs (the median redshift of galaxies detected in radio surveys is typically $z \approx 1$; Condon 1989).

At 1.4-GHz flux densities above about 50 mJy, more than 95 per cent of radio sources are classical radio galaxies and quasars powered by active galactic nuclei (AGN). Below 50 mJy, the AGN

★E-mail: ems@physics.usyd.edu.au

proportion declines and an increasing fraction of the faint radio source population is identified with star-forming galaxies (e.g. Condon 1989, 1992). These are usually disc galaxies, sometimes interacting with neighbours, in which the radio emission arises mainly through synchrotron emission from relativistic electrons accelerated by supernova explosions. Thus radio surveys to levels of a few mJy probe both the AGN population and a population of star-forming galaxies. It is important to be able to separate these, in order to determine the local space density and redshift evolution of each population.

A new generation of radio imaging surveys (NVSS, Condon et al. 1998; FIRST, Becker, White & Helfand 1995; WENSS, Rengelink et al. 1997; SUMSS, Bock, Large & Sadler 1999) is now covering the whole sky to sensitivities of a few mJy. Radio source counts from such surveys potentially yield important information on the cosmological evolution of active and star-forming galaxies (e.g. Longair 1966; Jauncey 1975; Wall, Pearson & Longair 1980), but their interpretation is strongly model-dependent. The scientific return from large radio surveys is enormously increased if the optical counterparts of the radio sources can be identified, their optical spectra classified (as AGN, starburst galaxy, etc.), and their redshift distribution measured. In the past, however, this was a slow and tedious process which could only be carried out for relatively small samples.

Now, fibre-fed optical spectrographs make it possible to carry out spectroscopy of complete samples of hundreds of thousands of galaxies in the local Universe. The Anglo-Australian Observatory's Two-degree Field (2dF) spectrograph can observe up to 400 galaxies simultaneously over a 2°-diameter region of sky (Lewis et al., in preparation; see also www.aao.gov.au/2df/). A Six-degree Field (6dF) spectrograph will be commissioned on the AAO's Schmidt Telescope in 2001, with 150 fibres over a 6°-diameter field, and in the northern hemisphere the Sloan Digital Sky Survey (SDSS) (York et al. 2000) has begun a programme of spectroscopy of 10^6 galaxies. Cross-matching radio continuum surveys with these new optical redshift surveys will provide redshifts and spectroscopic data for tens of thousands of local radio-emitting galaxies, rather than the few hundred available at present.

Two recent studies show the potential of these new redshift surveys. Machalski & Condon (1999, hereafter MC99) identified 1157 galaxies in the Las Campanas Redshift Survey (LCRS) with NVSS radio sources above 2.5 mJy at 1.4 GHz. They attempted to determine the radio and infrared properties of galaxies in the LCRS redshift range of $z = 0.05$ – 0.2 , but had difficulties because the LCRS was sparsely sampled, with optical spectra being taken for only about one galaxy in three. Nevertheless, Machalski & Godlowski (2000, hereafter MG) used the LCRS to derive the local radio luminosity function (RLF) for both AGN and star-forming galaxies, and to test for evolution over the LCRS redshift range.

Sadler et al. (1999, hereafter Paper I) cross-matched the NVSS radio catalogue with the first 30 fields observed in the 2dFGRS, and found that it was usually straightforward to tell from the optical spectra whether the radio emission arose from star formation or an AGN (unlike LCRS, the 2dFGRS has a spectroscopic completeness of 95 per cent).

The present paper is the second in a series analysing the properties of NVSS radio sources which are identified with galaxies in the 2dF Galaxy Redshift Survey (2dFGRS) (Colless 1999; Colless et al. 2001; see also www.mso.edu.au/2dfgrs/). When complete, the 2dFGRS will yield good-quality optical spectra for up to 4000 radio-emitting galaxies in the redshift

range $z = 0$ to 0.4 . Such a large sample should allow us to disentangle the effects of age, orientation and luminosity in the local AGN population, as well as providing a definitive measurement of the local RLF for active and star-forming galaxies. Our Paper I was a preliminary investigation of a small sample of the early 2dFGRS data, and showed that the 2dFGRS radio source population is composed of roughly similar numbers of AGN and star-forming galaxies. In this paper we analyse a 2dFGRS data set which is almost an order of magnitude larger than that in Paper I, and use it to derive the local RLF for active and star-forming galaxies at 1.4 GHz.

The spectra analysed in this paper are included in the first public release of 2dFGRS data, which took place in 2001 June.

Throughout this paper, we use $H_0 = 50 \text{ km s}^{-1} \text{ Mpc}^{-1}$ and $\Omega_0 = 1$.

2 SAMPLE SELECTION

In this paper we analyse 2dFGRS spectra from the first two years of the survey, i.e., up to 1999 May. Observations made before 1997 October were excluded, because the instrument was still in a commissioning phase and the data are of variable quality. The data set analysed here comprises 210 fields, or about 20 per cent of the total 2dFGRS area. The original selection of 2dFGRS optical targets included all non-stellar objects brighter than $b_J \approx 19.5$ from the photographic UKST Southern Sky Survey, and should involve no explicit biases so far as radio properties are concerned.

2.1 Area covered

The 2dFGRS uses a tiling algorithm with variable overlap depending on the underlying galaxy density. Some 2dFGRS fields are also shared with a parallel QSO redshift survey, so calculating the exact area of sky observed is not straightforward until the whole survey is complete.

We therefore use the method described by Folkes et al. (1999), and estimate the area of sky covered by dividing the number of galaxies observed by the mean surface density of galaxies in the target list. The data set observed in the period from 1997 October to 1999 May inclusive contains 58 454 2dFGRS targets. Taking the Folkes et al. surface density of $180 \text{ galaxies deg}^{-2}$ to the survey limit of $b_J = 19.45 \text{ mag}$ gives an effective area of 325 deg^2 for the data set we will analyse here.

2.2 Radio source identifications

We cross-matched the 2dFGRS catalogue positions with the NVSS radio catalogue, and took all matches with position offsets of 15 arcsec or less as candidate radio detections. This yielded a total of 927 observations of 903 targets. Not all these will be true identifications – as discussed in Paper I, we expect most unresolved radio sources with offsets of 10 arcsec or less to be true associations with 2dFGRS galaxies, along with a smaller (and quantifiable) fraction of sources with offsets of 10–15 arcsec.

There are also three classes of objects for which the situation is more complex: (i) extended (resolved) NVSS radio sources, (ii) radio sources which are resolved by NVSS into two or more distinct components, and (iii) radio sources associated with nearby bright galaxies ($b_J < 17 \text{ mag}$). As we discuss in Section 4, these received extra attention to determine whether to accept a candidate identification (ID) as a correct one.

For completeness, and because others may wish to use our data with different selection criteria for radio source IDs, we have tabulated 2dFGRS spectral types and redshifts for all 912 candidate radio source IDs with radio–optical offsets of 15.0 arcsec or less. We showed in Paper I that, with the exception of a small number of double NVSS radio sources (see Section 4.2), there should be very few correct IDs with radio–optical offsets larger than 15 arcsec. This is confirmed in Fig. 1, which shows that by 15 arcsec from the 2dF position the number of candidate detections falls to the level expected from chance coincidences alone.

We also note that the 2dFGRS input catalogue is incomplete for galaxies brighter than $b_J \approx 14$, and so some bright, nearby galaxies are missing from the 2dFGRS. Almost all these missing galaxies should already have redshift measurements, and can be added back into the sample once the entire 2dFGRS is complete. In calculating luminosity functions (see Section 8), we correct for the absence of these bright galaxies.

3 OPTICAL SPECTRA

As noted earlier, the spectra analysed in this paper were collected as the 2dFGRS progressed, and cover the period to 1999 May. Most of these spectra are included in the first (mid-2001) public release of 2dFGRS data (see Colless et al. 2001 for details of the public-release data base). In a few cases, a new spectrum taken after 1999 May may be better than the one used here and will replace it in the final data base.

Although in most cases the public-release data are identical to those analysed here, some values of b_J , z and Q listed in Table 1 may change. This is because there have been revisions of the b_J magnitude scale, and a re-reduction of all the early 2dFGRS redshifts, since we began our analysis. In the great majority of cases, the data base revisions produced no significant difference, especially for spectra with $Q \geq 3$. Small changes in the values of b_J or z for individual galaxies will not affect the overall results of the analysis which follows.

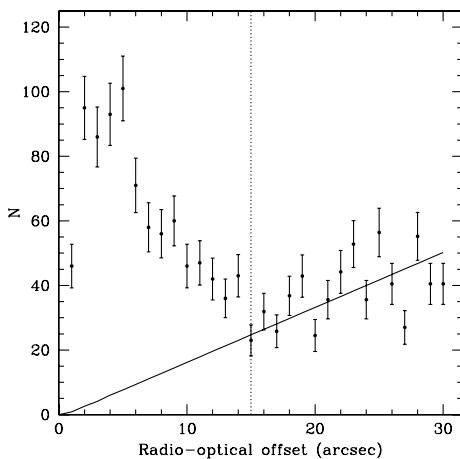


Figure 1. Number of candidate NVSS detections of 2dFGRS galaxies plotted against the offset Δ between radio and optical positions. The solid line shows the number of matches expected by chance from a sample of 58 454 2dFGRS galaxies, assuming that NVSS radio sources are randomly distributed on the sky with a surface density of 60 deg^{-2} . Note that at a separation of 15 arcsec or more, the number of matches declines to that which would be expected by chance, so we adopted a separation cut-off of 15 arcsec for candidate 2dFGRS radio sources.

3.1 Spectral classification

2dFGRS spectra of each of the 912 candidate radio source IDs were examined and classified visually by one of us (EMS). As in Paper I, each spectrum was classified as either ‘AGN’ or ‘star-forming’ (SF) based on its 2dF spectrum. AGN galaxies have either an absorption-line spectrum like that of a giant elliptical galaxy (these we classed ‘Aa’); an absorption-line spectrum with weak LINER-like emission lines (class ‘Aae’), or a stellar continuum dominated by nebular emission lines such as [O II] and [O III] which are strong compared with any Balmer-line emission (class ‘Ae’). ‘SF’ galaxies are those where strong, narrow emission lines of H α and (usually) H β dominate the spectrum. Objects where the spectra were too noisy for reliable classification are classed as ‘??’.

There are several independent tests of the reliability of our visual classification of the spectra: (a) the visual classifications generally agree well with the results of principal components analysis (PCA) methods, as we will show in Section 3.3, (b) for galaxies with optical emission lines, our Ae/SF classifications agree well with those derived by Jackson & Londish (2000) from diagnostic emission-line ratios, and (c) most galaxies that we classify as SF are detected by *IRAS* and fall on the radio–FIR correlation (see Section 6), whereas none of the galaxies we classified as Aa are detected by *IRAS*. Thus we are confident that our visual classification of the 2dFGRS spectra allows us to distinguish AGN and SF galaxies in a consistent and reliable way.

3.2 Data table

Table 1 lists the entire sample of 912 candidate radio IDs, i.e., the 903 2dFGRS targets whose catalogued position is within 15 arcsec of the catalogued position of an NVSS radio source, together with a further nine extended and double radio sources which were identified separately as described in Section 4.2. The full table is only available electronically in the on-line version of the journal on *Synergy*; a small subsample is reproduced in the printed journal for reference. The table columns are as follows.

- (1) 2dFGRS galaxy name (this is the name used in the 2dFGRS data base). An asterisk following the name indicates that this galaxy appears in the notes at the end of Table 1.
- (2) Other name – we have cross-identified with other galaxy catalogues where possible.
- (3) The optical position (J2000.0) at which the 2dFGRS fibre was placed.
- (4) The offset between 2dFGRS (optical) and NVSS (radio) positions, in arcsec.
- (5) Total blue (b_J) magnitude, from the 2dFGRS data base. The magnitudes listed here are taken from the 2000 May version of the data base.
- (6) Total radio flux density at 1.4 GHz, from the NVSS catalogue (Condon et al. 1998). Where a source is split into more than one component in the NVSS catalogue, this is indicated in the notes at the end of the table, and the value quoted here is the sum of all the components.
- (7) *IRAS* 60- μm flux density (in Jy), where listed in the NASA Extragalactic Database (NED). Although *IRAS* surveyed 97 per cent of the sky, the incompleteness near the Galactic poles is larger than in other areas. Based on the *IRAS* sky coverage plots given by Beichman et al. (1988), about 10 per cent of the 2dFGRS survey area had either one or no *IRAS* scans and so was not catalogued. The main 2dFGRS areas missed by *IRAS* lie in the region between

Table 1. Candidate 2dFGRS/NVSS radio sources. This is a sample – the full table is available in the on-line version of the journal on *Synergy*.

(1) 2dFGRS name	(2) Other name	(3) Position α (J2000) δ	(4) Offset (arcsec)	(5) b_J (mag)	(6) $S_{1.4}$ (mJy)	(7) $S_{60\mu m}$ (Jy)	(8) Redshift z	(9) Q	(10) Class	(11) Comments
TGS203Z262		00 16 41.06 – 26 51 18.2	6.7	15.37	4.8		0.0560	4	Aa	
TGS202Z238		00 17 15.53 – 26 39 29.2	0.9	18.12	90.5		0.1390	5	Aa	
TGS202Z085		00 17 38.37 – 27 22 15.3	2.1	18.68	6.4		0.1516	4	Aa	
TGS204Z164		00 20 35.49 – 27 51 44.6	0.9	19.41	57.7			2		
TGS203Z189		00 20 55.14 – 26 35 06.7	14.9	18.66	10.2		0.2283	4	Aa	Extended radio source – correct ID
TGS203Z019		00 22 01.41 – 27 33 23.0	2.5	18.86	85.1		0.2358	4	Aa	Extended radio source
TGS204Z102		00 23 47.45 – 27 56 14.4	1.8	16.79	3.2		0.0759	4	Aa	
TGS204Z037		00 25 54.06 – 27 23 30.4	1.8	19.41	54.0		0.2643	4	Aae	Extended radio source
TGS205Z218		00 29 06.95 – 27 05 36.9	12.2	16.26	2.5		0.0626	4	Aa	
TGS206Z164	ESO 410–013	00 29 55.72 – 27 29 50.6	8.8	14.58	2.9	0.293	0.0255	4	SF	
TGS206Z130		00 32 43.30 – 27 47 04.0	13.3	19.22	2.7		0.1484	4	Aa	
TGS206Z038		00 35 43.58 – 27 38 05.2	0.9	19.15	203.4		0.2424	4	Aa	Extended radio source
TGS206Z015		00 36 00.35 – 27 15 34.0	1.2	17.44	11.3	4.294	0.0700	4	SF	
TGS207Z011	ESO 410–024	00 36 27.41 – 27 47 07.0	0.2	14.19	55.0		0.0355	4	Ae	
TGS206Z005	ESO 410–025	00 36 37.33 – 27 47 20.8	11.8	15.23	3.7	0.217	0.0246	4	SF	Bright galaxy – correct ID
TGS284Z002		00 36 46.92 – 28 12 07.0	3.7	17.66	7.6		0.0988	4	Aa	
TGS206Z183		00 37 17.04 – 27 52 35.8	11.4	19.44	2.9		0.2402	4	Aa	
TGS208Z145	ESO 411–003	00 39 18.28 – 27 20 58.8	5.2	14.09	4.7	0.597	0.0229	4	SF	
TGS207Z112		00 40 23.20 – 27 58 38.2	4.4	16.94	3.0		0.1084	3	SF?	
TGS208Z104		00 41 10.99 – 27 51 06.5	0.9	19.05	16.3		0.2521	4	Aa	Extended radio source
TGS209Z223		00 45 20.11 – 26 57 27.0	0.4	16.98	8.7		0.1211	4	Aae	
TGS209Z218	IC 1579	00 45 32.41 – 26 33 55.2	2.1	14.01	4.1	0.240	0.0226	4	SF	
TGS288Z075		00 46 32.75 – 28 20 54.0	3.2	17.86	2.5		0.1935	4	Ae	
TGS209Z078*	ESO 411–011	00 46 40.74 – 27 53 54.5	6.0	15.89	3.5		0.0603	4	Aae?	
TGS209Z156		00 50 40.29 – 27 04 40.0	1.1	18.47	6.4	1.134	0.1289	4	SF	
TGS210Z205		00 51 21.18 – 26 59 21.7	4.8	16.05	4.8		0.0743	4	Aa	
TGS210Z106*		00 52 15.01 – 27 19 41.2	3.3	15.07	12.7		0.0400	4	SF	Extended radio source
TGS210Z188		00 53 08.98 – 27 08 11.5	7.6	18.98	17.7		0.1454	4	Aae?	Extended radio source
TGS210Z184	ESO 474–039	00 53 43.41 – 27 02 59.1	2.7	14.45	15.4	1.423	0.0183	4	SF	Extended radio source
TGS211Z020		00 58 52.32 – 28 18 11.7	1.8	15.55	3.1	0.377	0.0577	4	SF	
TGS212Z241		00 58 53.43 – 26 59 50.3	10.4	16.83	3.4	0.260	0.1064	4	SF	Bright galaxy – correct ID
TGS212Z217		01 01 48.13 – 26 42 41.8	13.7	19.14	2.6		0.1886	4	Aa	
TGS212Z209		01 02 15.31 – 26 33 21.9	7.1	19.14	3.1		0.2241	4	Aa	
TGS212Z069	ESO 412–003	01 03 46.31 – 27 45 13.3	4.4	15.11	7.6	0.542	0.0176	4	SF	
TGS292Z076		01 05 27.33 – 28 10 55.1	14.0	18.84	10.9		0.1882	4	Aa?	
TGS212Z046		01 05 31.65 – 27 29 43.4	7.2	18.24	3.0		0.1105	4	Aa	
TGS213Z017		01 11 19.84 – 27 52 49.1	12.1	18.90	5.7	0.199	0.1312	3		
TGS214Z124		01 12 49.62 – 27 54 41.8	13.5	17.62	5.0		0.1118	4	Aa?	
TGS215Z175		01 14 21.04 – 27 18 45.3	3.8	18.80	98.1			2		Extended radio source
TGS215Z170		01 14 48.43 – 28 01 17.8	1.4	18.77	23.5			2		

10^h and 11^h RA in the northern zone and 23^h and 0^h RA in the southern zone, but there are also smaller gaps elsewhere.

(8) Heliocentric redshift, from 2dFGRS observations unless otherwise indicated in the notes.

(9) 2dFGRS spectrum quality code Q, where $Q = 4$ or 5 are excellent-quality spectra, $Q = 3$ acceptable, and $Q = 0, 1$ or 2 poor-quality. Galaxies with $Q < 3$ are excluded from further analysis because their redshifts are highly uncertain. Checks against repeat observations and published redshifts show that 2dFGRS redshifts with $Q = 3$ are about 90 per cent reliable, and those with $Q = 4$ or 5 are 99 per cent reliable (Colless et al. 2001).

(10) Spectral class, based on our visual classification.

3.3 Comparison of visual and PCA spectral classifications

We would eventually like to compare the 2dFGRS radio-emitting galaxies with the parent sample from which they are drawn (in order to answer questions like ‘what fraction of Seyfert 1 and 2 galaxies are radio-loud, and how does this vary with redshift?’), so we compared our simple visual classification of the spectra (as Aa, Ae or SF) with the PCA methods developed for use with the 2dFGRS by Folkes et al. (1999) and Madgwick et al. (2001). PCA is an automatic method of classifying spectra which has the great advantages of being objective, quantitative and easily applied to very large samples. A series of principal components (PCs) or eigenspectra (PC1, PC2, ...) are determined from the distribution of all the spectra in a very large multidimensional space; most of the information in the spectra is included in the first few PCs. This means that each spectrum can be well represented by a set of just three or four numbers, corresponding to the relative power in the dominant PCs.

We find good agreement between the visual and automatic methods of classifying galaxy spectra. For example, in a plot of PC3 against PC1 (Fig. 2) there is a clear separation between the different visual spectral types. By combining similar plots involving PC2, it looks as if it will be possible to define an almost unique mapping between the two classification methods, making it easy to compare the properties of the 1.5 per cent of the galaxies which are radio sources with the full 2dFGRS sample of up to 250 000 optical galaxies.

3.4 Spectral class and redshift

Fig. 3 shows how the composition of the 2dFGRS radio sources changes with redshift. As we showed in Paper I, star-forming galaxies dominate the population at low redshift, while active galaxies dominate above $z \approx 0.1$. This is because star-forming galaxies are low-luminosity radio sources ($P_{1.4} < 10^{23} \text{ W Hz}^{-1}$), which drop out of the sample when they fall below the NVSS radio detection limit. Conversely, most AGN have higher radio luminosities and remain in the sample out to $z \approx 0.2\text{--}0.3$, where they finally drop below the 2dFGRS optical magnitude limit.

Interestingly, the fraction of emission-line AGN (Ae) galaxies remains roughly constant (at 10–15 per cent) throughout the sample volume, even though the overall AGN fraction increases dramatically with redshift. We need to keep in mind, however, that the 2-arcsec diameter 2dF fibres include an increasing fraction of the total galaxy light for more distant galaxies (see Fig. 4). As a result, galaxies with emission-line nuclei will be easier to recognize at lower redshift, where there is less dilution from the surrounding stellar galaxy, than at higher redshift. We therefore

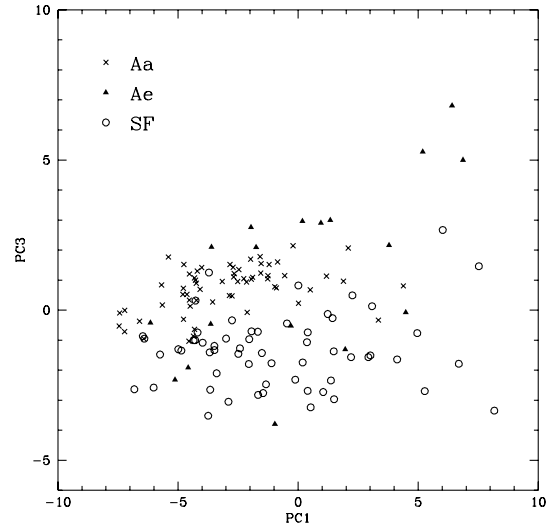


Figure 2. Plots of the first and third PCA components from 2dF spectra of radio-emitting galaxies. The three spectral classes from our visual classification are reasonably well separated in this plot, although some Ae galaxies overlap the region populated by SF galaxies. The PCA data used in this preliminary analysis were taken from an early version of the data base, and there have been some significant revisions of the PCA scheme since then (Madgwick et al. 2001).

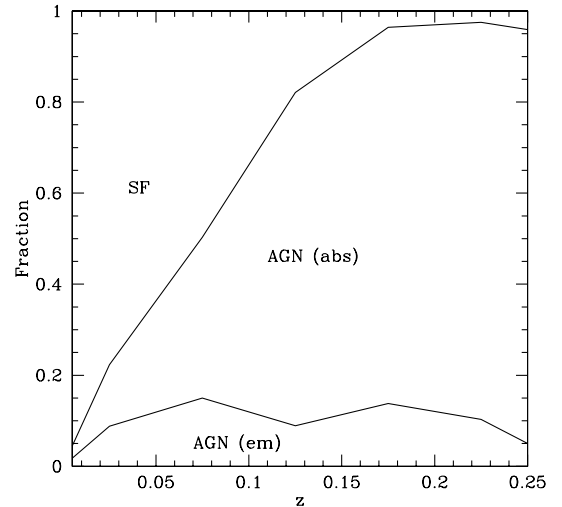


Figure 3. Change in spectral mix with redshift for 2dFGRS/NVSS galaxies. SF indicates star-forming galaxies with H II-region optical spectra, and AGN (em) and AGN (abs) indicate active galaxies with and without strong optical emission lines.

assume that the probability of recognizing a galaxy as Ae rather than Aa varies with redshift, and so we combine the Aa and Ae classes in most of our later analysis.

In star-forming galaxies, the line emission is expected to come mainly from an extended disc, and dilution of the emission-line flux with redshift is less likely. Indeed, we might expect star-forming galaxies to be easier to recognize at higher redshift, since the 2dF aperture includes a larger fraction of the total disc light.

4 RADIO–OPTICAL IDENTIFICATIONS

We now need to determine which of the candidate radio source

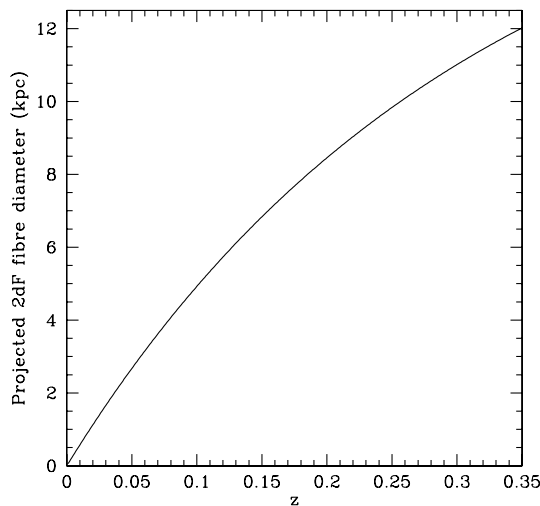


Figure 4. Projected diameter of the 2dF fibres (in kpc) for galaxies over the redshift range $z = 0$ to 0.35 .

identifications in Table 1 are real associations between a 2dFGRS galaxy and an NVSS radio source. This is not always straightforward – as noted in Paper I, we expect some chance coincidences even at the smallest radio–optical separations. In Paper I we used a simple 10-arcsec cut-off as the criterion for association. Although this will include a few objects that are not real associations and exclude some that are, the *number* of such objects can be quantified statistically and taken into account when calculating the luminosity function.

We use a similar 10-arcsec cut-off here, but also recognize that a simple cut-off may exclude some extended sources with complex radio structure. Thus we also inspected radio–optical overlays of all the extended sources in the candidate list, and accepted some of these as genuine IDs even though the radio–optical offset was larger than 10 arcsec.

4.1 Extended radio sources

About 25 per cent of the candidate NVSS/2dFGRS radio sources are resolved by the 45-arcsec NVSS beam, giving us an estimate of their linear size. In most such cases we still see a single radio source, but with an apparent size larger than 45 arcsec in at least one dimension. For these galaxies, the NVSS radio position is calculated by fitting a two-dimensional Gaussian to the radio image. If the fit is not perfect, the quoted position may have a much larger uncertainty than that of an unresolved radio source of similar flux density.

For all extended NVSS sources with radio–optical offsets in the range 10.0–15.0 arcsec, we inspected overlays of the radio contours on to DSS images (see Fig. 5 for examples). If the optical galaxy lay along the major axis of the extended radio source, or the radio emission appeared to be symmetric about the optical galaxy, we accepted this as a correct ID.

4.2 Double radio sources

A few NVSS radio sources are resolved into two or more distinct components, so we need to be able to recognize these, and to search for an optical ID near the radio centroid rather than at the position of each individual component.

We first identified all the candidate double radio sources in the

NVSS catalogue by using the semi-empirical link-length measure defined by Magliocchetti et al. (1998). A pair of radio sources are defined to be associated if

(i) the ratio of their flux densities S_1 and S_2 lies in the range $0.25 < (S_1/S_2) < 4.0$, and

(ii) the projected separation of the two radio components is smaller than their link length r , which is calculated from the total flux density in mJy and defined as

$$r = [(S_1 + S_2)/100 \text{ mJy}]^{0.5} \times 100 \text{ arcsec.} \quad (1)$$

This yielded a total of 525 candidate NVSS doubles in the 1700 deg^2 region of sky covered by the 2dFGRS. Of these, 59 had a 2dFGRS galaxy within 30 arcsec of the radio centroid, and 17 of these galaxies had spectra taken up to 1999 May. These objects were then inspected to see whether the optical galaxy lay on or near the radio axis of the NVSS double. As a result, eight new 2dFGRS galaxies were added to the sample as optical hosts of NVSS doubles. These are listed at the end of Table 1, along with an unusual diffuse source, tentatively identified with TGN307Z092, which is discussed in Section 5.2. These nine extra galaxies bring the total number of candidate NVSS/2dFGRS matches to 912 (of these, 56 per cent are AGN and 35 per cent SF galaxies).

4.3 Optically bright galaxies

We paid special attention to the brightest 2dFGRS galaxies ($b_J = 14.0\text{--}17.0 \text{ mag}$). For these bright galaxies, the radio–optical offset alone is not always a reliable indicator of whether the galaxy is associated with an NVSS radio source. There are three reasons for this: (i) it can be difficult to measure an accurate optical position for these galaxies from Schmidt plates, since the central regions are often overexposed, (ii) we found that the 2dFGRS fibre positions used for bright galaxies were sometimes offset from what appeared to be the optical nucleus, and (iii) much of the radio emission in these galaxies arises from star formation-related processes in a resolved disc (see Section 5 for more details), so that the centroid of the radio emission can be offset by several arcsec from the galaxy nucleus. We therefore inspected radio overlays on DSS images of all galaxies brighter than mag 17.0, and accepted those with 10.0–15.0 arcsec offsets as correct IDs if the radio emission appeared to be roughly centred on the optical galaxy. When this was done, it is noted in the final column of Table 1.

4.4 The final sample

Our final sample of accepted NVSS/2dFGRS IDs comprises all sources with radio–optical offsets of 10.0 arcsec or less, along with the nine additional double galaxies described above and 47 additional galaxies with radio–optical offsets of 10.0–15.0 (28 of them are radio sources associated with optically bright galaxies, and 19 are extended radio sources). This gives a final sample of 757 ‘accepted’ NVSS/2dFGRS IDs, which we use in further analysis.

Table 2 summarizes the spectral properties of the final sample. The 2dFGRS spectra are generally of excellent quality, allowing both the redshift and spectral class to be determined accurately. Of the 912 targets analysed here only 30 had spectra of quality class 1 or 2, i.e., were too noisy for a reliable redshift measurement. 18 targets turned out to be misclassified Galactic stars (i.e., had absorption-line spectra with $z < 0.001$), and two of the AGN were quasars (at redshifts $z = 1.5$ and 3.0).

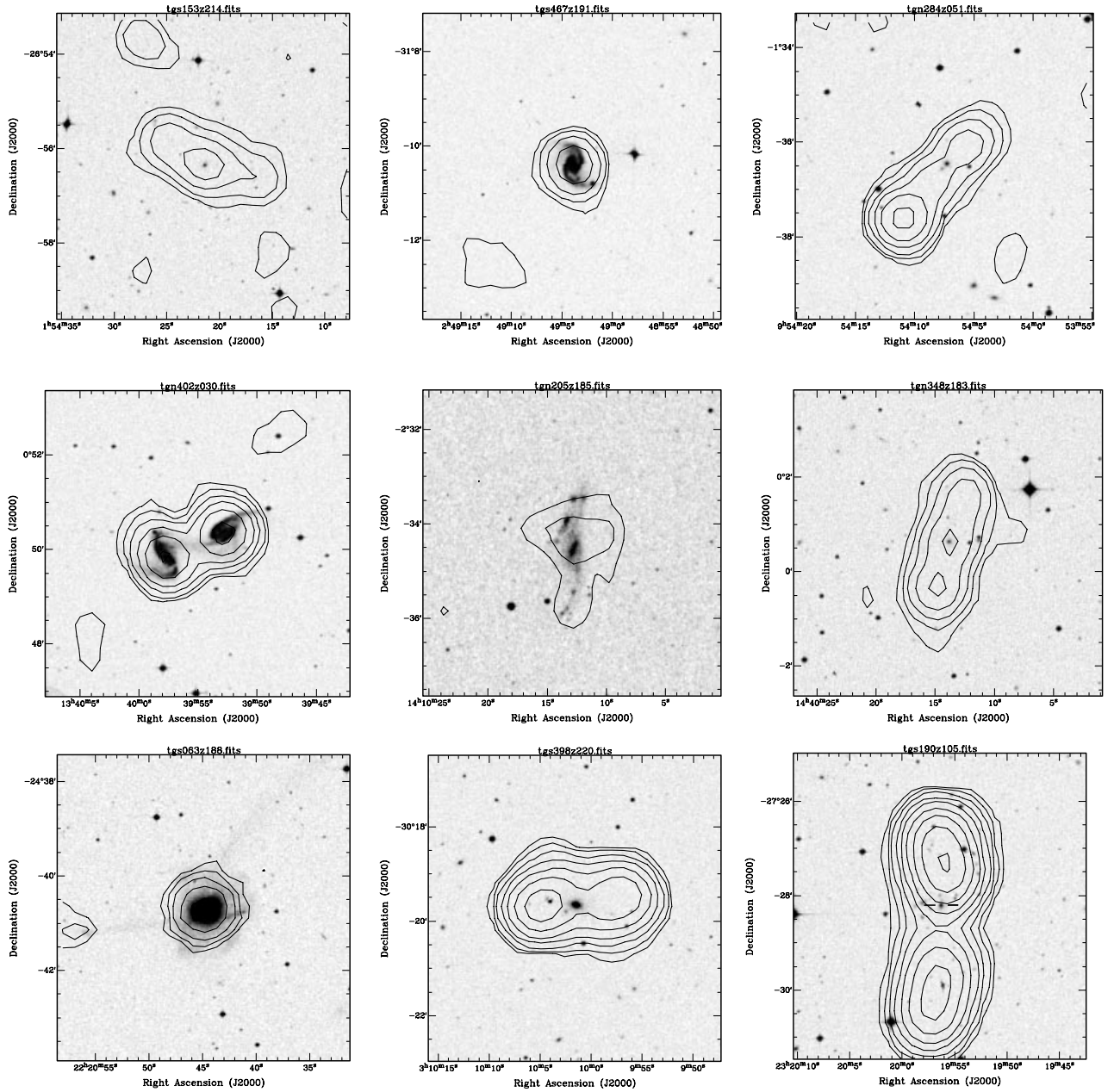


Figure 5. Overlays of NVSS radio contours on DSS optical images of some of the extended radio sources identified with 2dFGRS galaxies. Each frame shows a region 6.4 arcmin across. Contours are at 1, 2, 4, 8, 16, 32, ... mJy beam⁻¹, except for (h) TGS 398Z220 and (i) TGS 190Z105, where the lowest contour is at 4 mJy beam⁻¹. For TGS 190Z105, two dark lines mark the position of the faint galaxy identified as the radio source.

We can use the data presented in Fig. 1 to place some quantitative limits on the reliability and completeness of the final sample. We consider three zones in radio–optical offset Δ : (a) offsets below 10 arcsec, where all matches (other than Galactic stars) are accepted as correct IDs, (b) offsets of 10–15 arcsec, where we accept only a subset of matches (those associated with bright optical galaxies or extended radio sources, where an eye inspection suggests that the match is a correct one), and (c) offsets greater than 15 arcsec, which are rejected as correct IDs.

In the first zone ($\Delta < 10$ arcsec) there are 712 matches, and we include 702 of these in the final sample. However, integrating under the line in Fig. 1 implies that ~ 75 of these are likely to be chance coincidences. In the second zone ($\Delta = 10$ –15 arcsec) there are 191 matches, of which 47 are included in the final sample. We

expect 106 chance coincidences, suggesting that the final sample should contain ~ 85 objects in this zone, rather than the 47 which are actually included. Thus our selection criteria have probably excluded some genuine IDs in this zone. In the third zone ($\Delta = 15$ –30 arcsec) there are 590 matches, all of which we reject (we do, however, include eight NVSS extended double radio sources, which were selected separately as described in Section 4.2). Integrating under the line in Fig. 1 implies that we expect ~ 575 chance coincidences in this zone, suggesting that there are few or no ‘missing’ sample members in this zone.

In summary, we estimate that our final sample of 757 radio source IDs includes ~ 75 objects which are chance coincidences of an 2dFGRS galaxy and a background radio source, and is missing ~ 40 genuine radio-emitting galaxies which should have been

Table 2. Summary of spectral classifications for the galaxies listed in Table 1.

	All candidates	Accepted as ID	Rejected as ID
AGN	514	441	73
SF	319	272	47
Stars	18	0	18
Low S/N spectra	61	44	17
Total	912	757	155

included. Thus the sample is currently about 95 per cent complete and 90 per cent reliable (and the overall sample size is within 5 per cent of the correct value). In principle, both the completeness and the reliability could be raised to almost 100 per cent by measuring more accurate radio positions for the weaker ($S < 5$ mJy) radio sources in Table 1, and this will be done in the future.

4.5 Radio stars?

As noted above, our final sample of radio source IDs rejected all the NVSS–2dFGRS matches which had spectra characteristic of Galactic stars (with redshifts $z < 0.001$). As can be seen from Table 2, 18 of the 155 rejected IDs (12 ± 3 per cent) are Galactic stars. This is roughly twice the number expected for objects drawn at random from the 2dFGRS data set (6 per cent of the 2dFGRS objects observed up to 2001 March were Galactic stars; Colless et al. 2001), posing the question of whether we have detected any Galactic radio stars.

At first glance, this seems unlikely. Searches for radio stars in the NVSS and FIRST radio surveys (Condon, Kaplan & Yin 1997; Helfand et al. 1999) find a very low detection rate at high Galactic latitudes (both studies find less than one radio-detected star per 200 deg² for $V < 10$ mag, and Helfand et al. note that the detection probability drops steeply at fainter magnitudes).

Furthermore, the 2dFGRS stars are not randomly selected stars, but stars which have been misclassified as galaxies. Thus some of them are likely to be the chance superposition of a galaxy and a foreground star. At least one object in Table 1 (TGN 156Z046) certainly falls into this class – it was originally classified as a star with $z = 0.0005$, but examination of the spectrum showed that although the blue end of the spectrum was dominated by light from a foreground star, a higher redshift system at $z = 0.0391$ with emission lines of H α , [N II] and [S II], and Mg and NaD absorption lines, could be seen clearly at the red end.

Nevertheless, the superposition of galaxies and foreground stars is unlikely to provide a complete explanation for a larger-than-expected number of NVSS sources matched with Galactic stars, because it is hard to understand why radio-emitting galaxies should be more likely than other 2dFGRS galaxies to be obscured by foreground stars. It will be interesting to see whether the ‘radio star’ excess persists as the 2dFGRS data set grows. If so, it is possible that there may be a rare and so-far unrecognized class of radio sources associated with faint ($b_J > 16$ mag) Galactic stars.

4.6 Other identification criteria

MC99 took a different approach to cross-identifying NVSS radio sources with optical galaxies, and calculated a probability of association based on the radio–optical offset and the quoted errors in radio and optical positions. They considered all NVSS radio

sources within 30 arcsec of an LCRS galaxy, and calculated a normalized offset

$$\rho = [(\Delta_\alpha/\sigma_\alpha)^2 + (\Delta_\delta/\sigma_\delta)^2]^{0.5}, \quad (2)$$

where Δ_α and Δ_δ are the differences between radio and optical positions, and σ_α and σ_δ are the combined errors in the quoted radio and optical positions. They accepted a candidate identification as a true ID if $\rho < 2.5$. This method has the advantage that it allows a larger search radius for objects with larger position errors, but the disadvantage is that the probability of finding a spurious optical ID is larger for faint sources because of the larger error box.

We looked at the effect of applying the MC99 identification criterion to our own sample. Of the 695 unresolved sources in Table 1, 543 are identified as IDs by both criteria (i.e., MC99 and our own procedure as described above). 41 sources are rejected by both criteria, 38 are accepted by us but rejected by MC99, and 73 are accepted by MC99 but rejected by us. Thus the MC99 criterion produces about 6 per cent more IDs than our method for the same data set. This is probably not surprising – we know that our method excludes a few genuine IDs with large radio–optical separation in order to produce a sample which is as uncontaminated by chance coincidences as possible.

4.7 K -corrections

The galaxies in our sample have redshifts as high as $z = 0.3$ to 0.4, so when calculating galaxy luminosities we need to apply optical, radio and infrared k -corrections to take proper account of the effects of redshift on both the observed flux and the width of the passband.

In the optical, we follow Folkes et al. (1999) and adopt the B -magnitude k -corrections tabulated by Pence (1976), using Pence’s E/S0 values for our Aa and Ae galaxies, and the Sbc values for our SF galaxies. We also convert Pence’s $k(B)$ values to $k(b_J)$ using the relation

$$k(b_J) = k(B) - 0.28[k(B) - k(V)]. \quad (3)$$

In the radio, we assume a mean spectral index of $\alpha = -0.7$ (where $S \propto \nu^\alpha$) and apply the usual k -correction of the form

$$k(z) = (1 + z)^{-(1+\alpha)} \quad (4)$$

at redshift z .

In the far-infrared, the situation is more complex because of the wide range in *IRAS* ‘spectral index’ (i.e., dust temperature) observed in these galaxies (see Section 6). Because the FIR k -correction can be either positive or negative depending on what assumptions are made about the spectral energy distribution, and because many of our galaxies are weak *IRAS* sources with detections in only one or two bands, we chose to apply no k -correction when calculating FIR luminosities. Since most of the FIR-detected galaxies we will study are at low redshift ($z < 0.15$), the k -correction has little or no effect in any case.

5 RADIO STRUCTURES OF RESOLVED GALAXIES

About 25 per cent of the radio sources associated with 2dFGRS galaxies are spatially resolved by NVSS, allowing us to measure their projected linear size. In a few cases we remeasured the angular size ourselves (usually because the NVSS source catalogue split a single source into several components), otherwise

we used the NVSS catalogue value. Fig. 5 shows some of the extended NVSS sources identified with AGN and star-forming galaxies.

Fig. 6 plots radio power against projected linear size for the 182 extended NVSS radio sources with good-quality 2dFGRS spectra (i.e., with $Q \geq 3$ in Table 1). As expected, most star-forming galaxies are associated with radio sources less than about 60 kpc in diameter, i.e., no larger than a galaxy disc. The few star-forming galaxies whose radio extent is larger than this appear to be members of pairs or close groups in which more than one galaxy contributes to the radio emission. In contrast, many of the radio sources with AGN spectra are several hundred kpc in extent, consistent with classical (core plus jet) radio galaxies.

5.1 Giant radio galaxies

Our sample includes three giant radio galaxies with projected linear sizes greater than 1 Mpc, which are shown in Fig. 7. Two are newly discovered GRGs – TGS223Z232 ($z = 0.2095$) and TGS190Z081 ($z = 0.2318$). The third, TGS241Z299, corresponds to the radio galaxy MRC B0312–271 ($z = 0.2186$), which has already been identified as a GRG by Kapahi et al. (1998).

About 50–60 GRGs are currently known (Ishwara-Chandra & Saikia 1999; Schoenmakers et al. 2000) – they are believed to represent the last stages of radio galaxy evolution, and to be unusually old or long-lived radio sources. The three GRGs in our sample represent just under 1 per cent of the 441 AGN accepted as radio source IDs, so they are clearly rare. It would be interesting to determine whether there is anything different about their environment (e.g., low density, lack of recent interactions with companions) which has allowed these radio sources to grow undisturbed to such a large size.

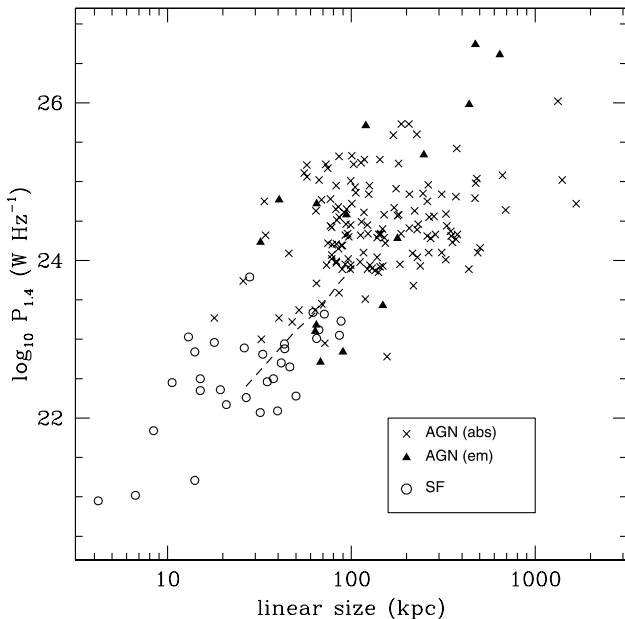


Figure 6. Relationship between radio power and projected linear size for spatially resolved 2dFGRS/NVSS radio sources. The dashed line shows the locus of a source with an observed angular size of 20 arcsec and flux density 2.5 mJy over the redshift range $z = 0.05$ – 0.3 . Most of the upper limits for unresolved sources fall to the left of this line. Sources larger than about 100 kpc will be resolved throughout the 2dFGRS sample volume.

5.2 Unusual radio sources

Fig. 8 shows two unusual radio sources discovered in our data set. The diffuse radio source shown in Fig. 8(a) is resolved into four separate components in the NVSS catalogue, and one of these was originally picked up as a possible match for the 2dFGRS galaxy TGN307Z090. Inspection of the radio contours showed that this is a large (~ 6.5 arcmin diameter) source with very low radio surface brightness.

The source is clearly real, since it was independently detected at Green Bank (also at 1.4 GHz) by White & Becker (1992). The single-dish flux density of 189 mJy suggests that NVSS may have missed some flux. At present, nothing is known about the radio spectral index. While the identification is uncertain at this stage, the radio centroid is closer to the 2dFGRS galaxy TGN307Z092 than to its companion TGN307Z090, so we tentatively identify the source with TGN307Z092. At the redshift of TGN307Z092 ($z = 0.0465$), the source has a projected linear size of 310 kpc and a 1.4-GHz radio power of $1.3 \times 10^{24} \text{ W Hz}^{-1}$. Its radio surface brightness is, however, unusually low. The nature of the source remains uncertain, although it may be a relic radio galaxy whose central engine has turned off (e.g. Komissarov & Gubanov 1994).

Fig. 8(b) shows the radio emission associated with the 16th-magnitude star-forming galaxy TGS 119Z122 at $z = 0.0090$. The NVSS flux density at 1.4 GHz is 11.7 mJy. However, the same object is listed in the Parkes catalogue as PKS 2225–253, with flux densities of 230 and 130 mJy at 2.7 and 5.0 GHz respectively. The Parkes observations were made by Wall, Wright & Bolton (1976), and the observing dates are given by them as 1974.0 and 1974.8 for the 2.7- and 5.0-GHz observations respectively. Thus the source was detected at two different frequencies and on two different occasions separated by several months, and appears to have been real. The optical identification with a 16th-magnitude galaxy was first made by Savage & Wall (1976).

The radio luminosity of PKS 2225–253 has declined dramatically since the 1974 Parkes observations. One possibility, since TGS 119Z122 is actively forming stars, is that the bulk of the Parkes emission came from a radio-loud supernova like SN 1986J or SN 1998Z (e.g. Weiler et al. 1998), which has since faded. However, the early Parkes observations imply a 5-GHz radio power around $4 \times 10^{22} \text{ W Hz}^{-1}$, which is 3 times higher than the peak luminosity of any known radio supernova, including the gamma-ray burst object SN1998bw (Kulkarni et al. 1998). A transient Galactic radio source seems unlikely at $b = -58^\circ$, and the nature of the catalogued Parkes source remains unclear.

6 IRAS DETECTIONS AND STAR-FORMING GALAXIES

6.1 IRAS detections of 2dFGRS galaxies

In the well-known correlation between far-infrared (FIR) and radio continuum emission in star-forming galaxies (e.g. de Jong et al. 1985; Helou, Soifer & Rowan-Robinson 1985), the FIR/radio ratio $S_{60\mu\text{m}}/S_{1.4\text{GHz}}$ has a mean value of ~ 105 (Condon & Broderick 1988). By a happy coincidence, this is very close to the ratio between the 280-mJy limit of the IRAS Faint Source Catalogue (FSC) (Moshir et al. 1990) at 60 μm and the 2.5-mJy detection limit of the NVSS at 1.4 GHz. As a result, we expect most star-forming galaxies detected as radio sources by NVSS to be detected as 60- μm sources in the IRAS FSC, and vice versa.

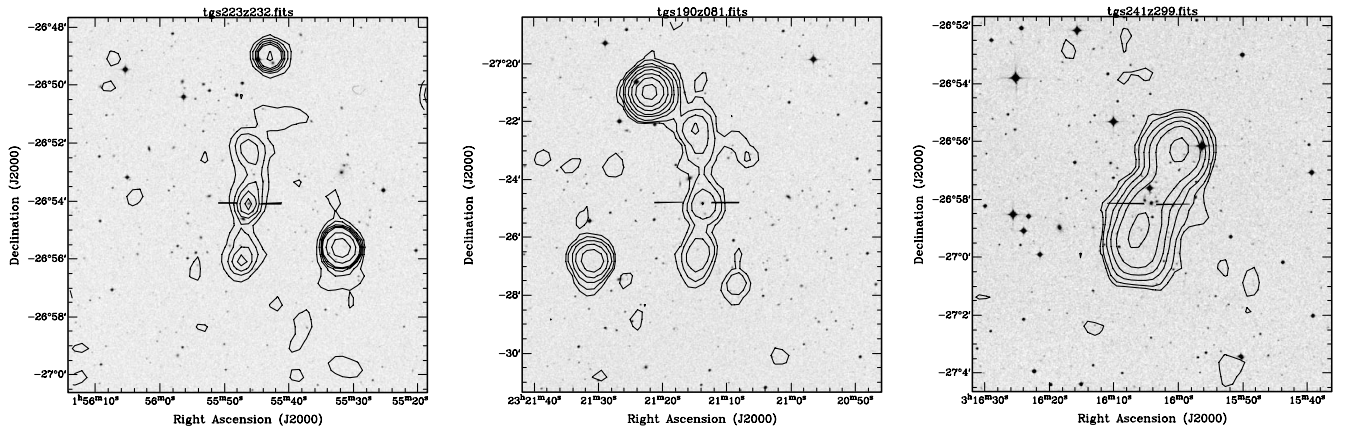


Figure 7. Radio contours overlaid on DSS optical images of the three giant radio galaxies (GRGs) detected in our sample: (a) TGS 223Z232 (contours 1, 2, 3, 4, 5, 10, 20, 50 mJy beam⁻¹), (b) TGS 190Z081 (contours 1, 2, 4, 8, 16, 32, 64, 128 mJy beam⁻¹), (c) TGS 241Z299 (contours 1, 2, 5, 10, 20, 50 mJy beam⁻¹). Each frame is 12.8 arcmin across.

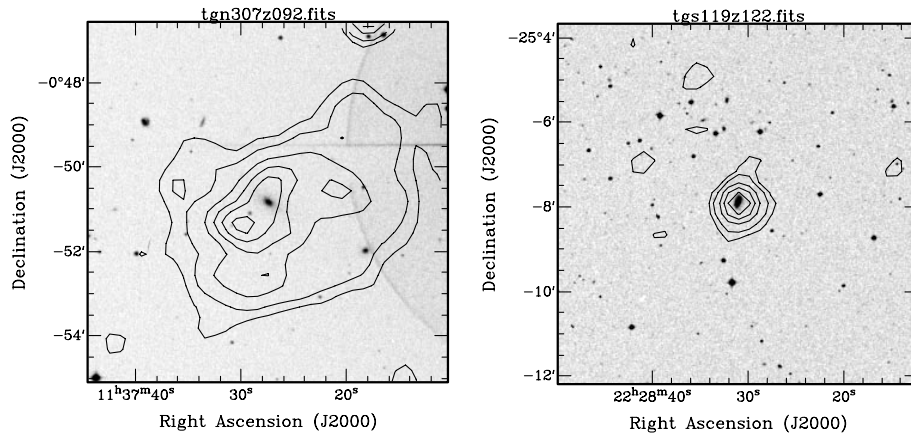


Figure 8. Radio contours overlaid on DSS optical images of two unusual radio sources in our sample. Each frame is 8.6 arcmin across. (a) Overlay of NVSS radio contours on a DSS image of TGN 307Z092 and its fainter companion TGN 307Z090 (contour levels 1, 2, 3, 4, 6, 8, 10, 12 mJy beam⁻¹), (b) NVSS contours overlaid on an image of TGS 119Z122 (PKS 2225–253; contour levels 1, 2, 4, 6, 8 mJy beam⁻¹).

In practice, as noted earlier in Section 3.2, about 10 per cent of the 2dFGRS survey region was either unobserved by *IRAS* or had only single-scan coverage. Thus the absence of an individual galaxy from the *IRAS* catalogue does not necessarily mean that it has a 60- μ m flux below the FSC limit.

Table 3 summarizes the spectral properties of the 183 accepted radio source IDs from Table 1 that were also detected at 60 μ m by *IRAS*. Most galaxies detected at 60 μ m (83 per cent) were also detected by *IRAS* at 100 μ m.

All the 2dF spectra of galaxies detected as *IRAS* sources show optical emission lines, in agreement with earlier studies (e.g. Allen, Roche & Norris 1985; Lawrence et al. 1986). The great majority (89 per cent) are classified as SF, with the remainder (11 per cent) being emission-line AGN with Seyfert-like spectra.

Extrapolating from our current sample suggests that the full 2dFGRS data base, when complete, will contain spectra of ~ 1000 *IRAS* galaxies. While this is smaller than targeted redshift surveys such as the *IRAS* PSCz (Saunders et al. 2000), which has more than 15 000 redshifts, it reaches to lower *IRAS* flux densities (and a higher median redshift) than most earlier surveys, as can be seen from Fig. 9. Since the general properties of *IRAS* galaxies are already well explored by earlier studies, we focus here on the radio properties of star-forming galaxies in the 2dFGRS.

6.2 The FIR–radio correlation

We calculated the FIR luminosity for each galaxy detected by *IRAS*, using the FIR flux defined by Helou et al. (1985):

$$S_{\text{FIR}} = 1.26 \times 10^{-14} \times (2.58S_{60} + S_{100}), \quad (5)$$

where S_{60} and S_{100} are the 60- and 100- μ m flux densities in Jy ($1 \text{ Jy} = 10^{-26} \text{ W Hz}^{-1} \text{ m}^{-2}$), and S_{FIR} is in W m^{-2} .

Fig. 10 plots FIR luminosity versus 1.4-GHz radio power for the *IRAS*-detected galaxies in our sample. Most galaxies fall close to the FIR–radio correlation for normal galaxies derived by Devereux & Eales (1989),

$$\log_{10} P_{1.49} = 1.28 \log_{10} L_{\text{FIR}} + 8.87, \quad (6)$$

but the scatter increases strongly for the most luminous galaxies.

As can be seen from Table 4, the fraction of galaxies with AGN-like optical spectra increases with FIR luminosity, and so it seems likely that the increased scatter in the FIR–radio correlation results from an increasingly diverse mix of pure star-forming galaxies and AGN or composite objects at higher FIR luminosities.

Table 3. Summary of spectral classifications for radio source IDs which were also detected by *IRAS*.

2dF spectral class	Galaxies
SF	161
Ae	16
Aae	5
Low S/N	1
Total	183

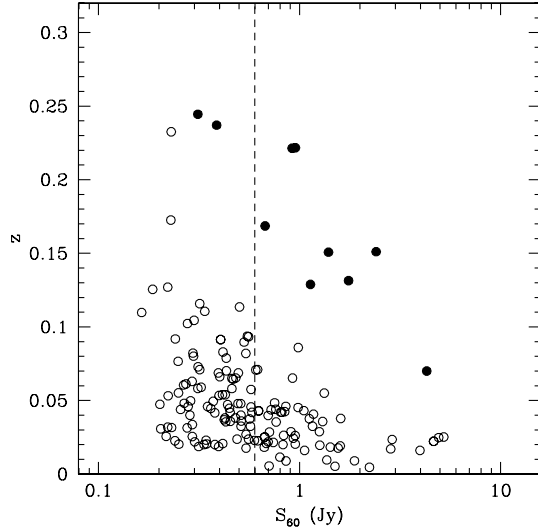


Figure 9. Plot of *IRAS* 60- μ m flux density versus redshift for *IRAS*-detected 2dFGRS radio sources. ULIRGs with $L_{\text{FIR}} > 10^{12} L_{\odot}$ are shown by filled circles, and other galaxies by open circles. The vertical line at 0.6 Jy corresponds to the flux limit of the PSCz survey (Saunders et al. 2000).

6.3 *IRAS* colours and 2dF spectral types

As noted by de Grijs et al. (1985), galaxies with active nuclei tend to have hotter *IRAS* colours (as measured by the flux ratio S_{60}/S_{100}) than ‘normal’ star-forming galaxies, and galaxies with Seyfert nuclei generally have $S_{60}/S_{100} > 0.5$.

Fig. 11 shows a FIR ‘colour–magnitude diagram’ for galaxies in our sample. The *IRAS* flux densities for weaker sources have typical errors of 10–15 per cent, so the *IRAS* colours can have uncertainties of 30 per cent or more. However, there is still a general increase in the fraction of galaxies with ‘hot’ *IRAS* colours at higher FIR luminosity (see also the summary in Table 4), consistent with an increasing contribution from active nuclei at higher FIR luminosity.

6.4 Ultraluminous *IRAS* galaxies

10 of the *IRAS* galaxies in our sample (listed in Table 5) have FIR luminosities above $10^{12} L_{\odot}$, and can be considered ‘ultraluminous *IRAS* galaxies’ (ULIRGs) (e.g. Sanders & Mirabel 1996). Most of these galaxies are already known as ULIRGs from other surveys, but there are two newly discovered ULIRGs, TGN 152Z171 and TGN 131Z280. Fig. 12 shows their spectra.

All the galaxies in Table 5 have unresolved radio sources in the NVSS, although because of the relatively large distances of these

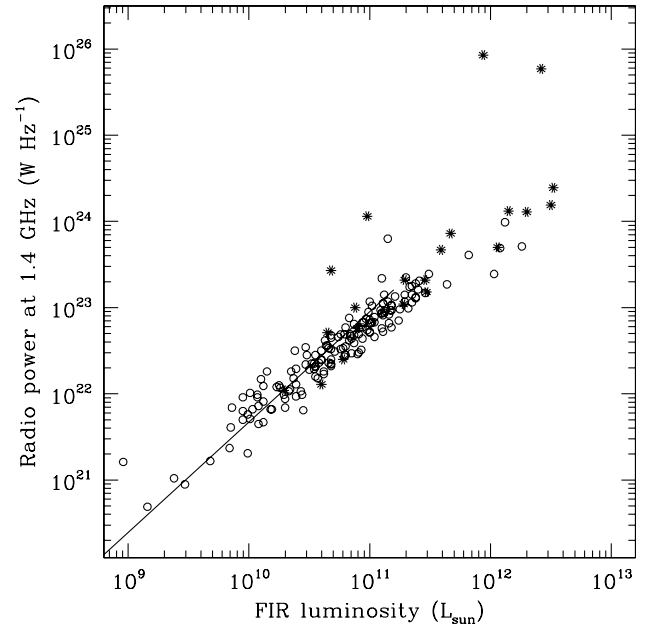


Figure 10. Relation between FIR and radio continuum luminosity for radio source IDs from Table 1. Galaxies with SF spectra are shown as open circles, and those with AGN spectra as stars. The solid line shows the FIR–radio correlation for normal galaxies derived by Devereux & Eales (1989). Note that because of the requirement that they lie above the 2.8-mJy NVSS detection limit, most of our 2dFGRS star-forming galaxies have star formation rates which are significantly higher than the majority of ‘normal’ galaxies.

Table 4. Summary of spectral properties for three bins in FIR luminosity. Hot *IRAS* galaxies are those with $\log_{10}(S_{60}/S_{100}) > -0.3$ (de Grijs et al. 1985).

$\log_{10}(L_{\text{FIR}})$ (L_{\odot})	Fraction with AGN spectra		Fraction with hot <i>IRAS</i> colours	
> 11.5	60%	(9/15)	92%	(11/12)
$10.5-11.5$	9%	(11/118)	46%	(45/99)
< 10.5	2%	(1/49)	27%	(11/41)

galaxies this only sets fairly unrestrictive limits (typically 100–200 kpc) on the linear size of the associated radio emission.

7 ROSAT DETECTIONS

Bauer et al. (2000) have cross-matched the NVSS source catalogue with the *ROSAT* Bright Source Catalogue (RSBC) of X-ray sources (Voges et al. 1999). They showed that the relatively low surface density of NVSS sources allows reliable identification of the radio counterparts of RSBC sources, despite uncertainties of 10 arcsec or more in the X-ray positions. The more accurate radio positions then allow a reliable optical identification to be attempted. Bauer et al. showed that the RSBC/NVSS radio sources were dominated by AGN with an average redshift of $\langle z \rangle \approx 0.1$.

We cross-matched the galaxies in Table 1 with the *ROSAT* All-Sky Survey (RASS) catalogue, taking a simple cut-off of 30 arcsec as our matching radius rather than the more complex criteria prescribed by Bauer et al. (2000). This gave the six matches listed in Table 6, four of which are also in the Bauer et al. list (the other

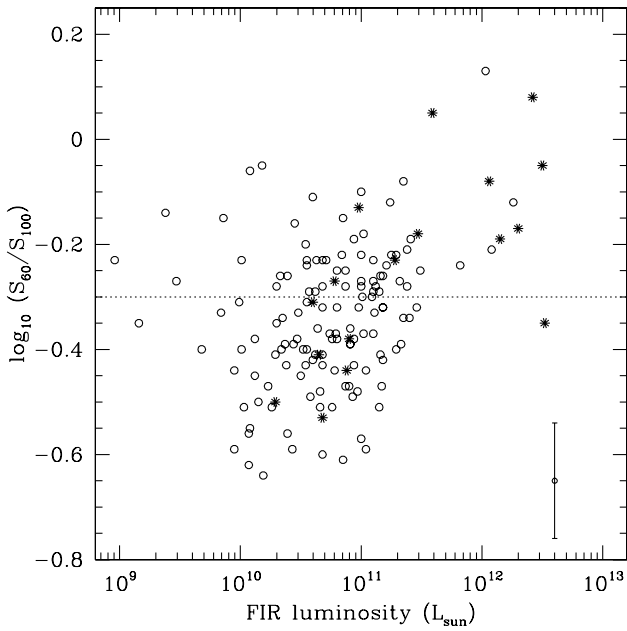


Figure 11. Plot of *IRAS* ‘colour’ [$\log_{10}(S_{60}/S_{100})$] versus FIR luminosity for galaxies in our sample. ‘Warm’ galaxies are defined by de Grijs et al. (1985) as those with $S_{60} > 0.5S_{100}$, and they find that most Seyfert galaxies have ‘warm’ *IRAS* colours. The boundary between warm and cool galaxies as defined by de Grijs et al. is shown by the dotted horizontal line, and a typical error bar for the weakest *IRAS* sources ($S_{60} \approx 0.3$ Jy) is shown in the lower right-hand corner. As in Fig. 10, open circles and stars denote galaxies classified spectroscopically as SF and AGN respectively.

two fall below the 0.1 count s^{-1} X-ray limit imposed by Bauer et al. for their sample).

All six galaxies in Table 6 have strong emission lines and spectra classed as Ae, but in other respects they are a diverse population, including three powerful, double-lobed radio galaxies, two Seyfert 1 galaxies with less powerful radio emission, and one ultraluminous *IRAS* galaxy (ULIRG) (see Table 5 and Fig. 13).

Bauer et al. (2000) identified 1512 extragalactic RSBC/NVSS sources with Galactic latitude $|b| > 15^\circ$ in the 10.3-sr NVSS survey area. This corresponds to a surface density of about 0.05 objects per square degree, or about 4 times higher than the corresponding surface density derived from the RSBC/NVSS/2dFGRS objects in Table 6 (0.012 objects per square degree).

Where are the missing RSBC/NVSS objects? We expect most of them to fall within the 2dFGRS volume, since Bauer et al. (2000)

note that their objects are mostly local with a mean redshift of about 0.1. Closer examination of the Bauer et al. objects in the 2dFGRS area suggests that about half the missing objects are bright, nearby galaxies that were excluded from the 2dFGRS. Most of the remainder appear to be Seyfert galaxies excluded because of their compact, stellar appearance on sky survey plates, along with a few higher redshift QSOs.

8 THE LOCAL RADIO LUMINOSITY FUNCTION (RLF) AT 1.4 GHz

8.1 Calculation of the local RLF

We now calculate the radio luminosity function (RLF) for 2dFGRS–NVSS galaxies with $z \leq 0.3$, both for the sample as a whole and for the AGN and SF subclasses. We assigned spectral types to the 19 unclassified galaxies with measured redshifts as follows: galaxies with b_J fainter than magnitude 17.0 and radio power above $10^{23} \text{ W Hz}^{-1}$ were assigned to the Aa (absorption-line AGN) class, otherwise they were assumed to be star-forming (SF). Using these criteria, we classify 18 of the low S/N galaxies as Aa and only one as SF.

To calculate the local RLF, we use the $1/V_{\text{max}}$ method (Schmidt 1968), as discussed by Condon (1989). V_{max} is calculated from the joint optical and radio limits of the sample, i.e., a radio cut-off of 2.8 mJy and optical cut-offs at $b_J = 14.0$ mag (bright) and 19.4 mag (faint). Table 7 lists the derived local RLF for the whole sample, and for the AGN and SF classes separately. At this stage, we make no corrections for incompleteness and the only normalization is the effective area of 325 deg^2 derived in Section 2.1.

Fig. 14 shows the derived RLF, together with earlier values derived by Condon (1989) and MG. An advantage of the 2dF/NVSS sample is that all the data are drawn from a single radio survey and a set of homogeneous optical spectra from a single instrument. Most previous determinations of the local RLF used data from several radio surveys to span the equivalent range in radio power. The good overall agreement with earlier derivations confirms our earlier calculation that the incompleteness in our final sample is small (< 10 per cent).

8.2 Comparison with earlier work

Figs 14 and 15 shows a comparison between our values of the local RLF and those derived by MG for a sample of 1157 radio-identified galaxies from the LCRS. This is the only other determination

Table 5. Ultraluminous *IRAS* Galaxies (ULIRGs) in the sample.

2dFGRS name	<i>IRAS</i> name	Spectral class	z	Abs. mag.	$\log_{10} P_{1.4}$ (W Hz^{-1})	$\log_{10} S_{60}/S_{100}$	$\log_{10} L_{\text{FIR}}$ (L_\odot)	Notes
TGS206Z015	IRAS 00335–2732	SF	0.0700	−20.71	23.39	0.13	12.03	S92; Megamaser
TGS209Z156	IRAS 00482–2720	SF	0.1289	−21.04	23.69	−0.21	12.08	K98, V99, C99
TGS238Z241	IRAS 03000–2719	Ae	0.2214	−22.52	24.39	−0.35	12.52	C96
TGN152Z171	IRAS F09521–0400	Ae	0.2371	−22.03	24.12	−0.19	12.15	New ULIRG
TGN314Z018	IRAS 11598–0112	Ae	0.1511	−22.01	24.19	−0.05	12.50	S92; <i>ROSAT</i>
TGN131Z280	IRAS 12532–0322	Ae	0.1686	−22.18	23.70	−0.08	12.06	New ULIRG
TGN137Z043	IRAS 13270–0331	Ae	0.2217	−22.16	25.77	0.08	12.42	C95
TGN206Z237	IRAS 14121–0126	Ae	0.1508	−21.35	24.11	−0.17	12.30	C95
TGS178Z172	IRAS 22206–2715	SF	0.1314	−21.98	23.71	−0.12	12.26	C96
TGS180Z060	IRAS F22301–2822	SF	0.2445	−21.92	23.99	> -0.47	12.12	C96

References: C95: Clowes et al. (1995); C96 Clements et al. (1996); C99 Clements et al. (1999); K98 Kim & Saunders (1998); S92: Strauss et al. (1992); V99 Veilleux et al. (1999).

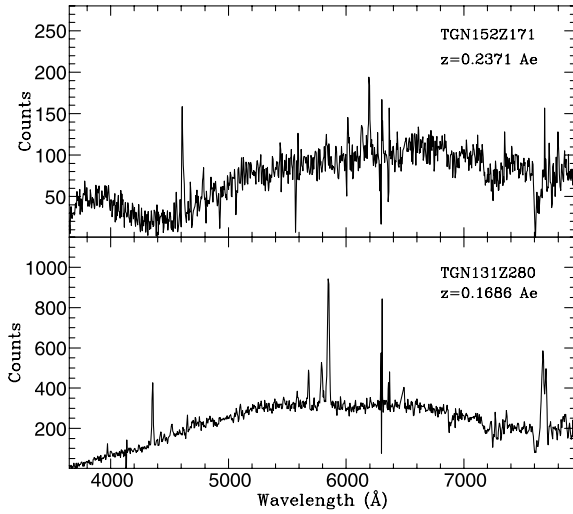


Figure 12. 2dFGRS spectra of the two newly discovered ULIRGs in our sample, TGN152Z171 ($B_J = 18.85$) and TGN131Z280 ($B_J = 17.93$). Both spectra show residuals due to incomplete subtraction of the atmospheric airglow line at 6300 Å.

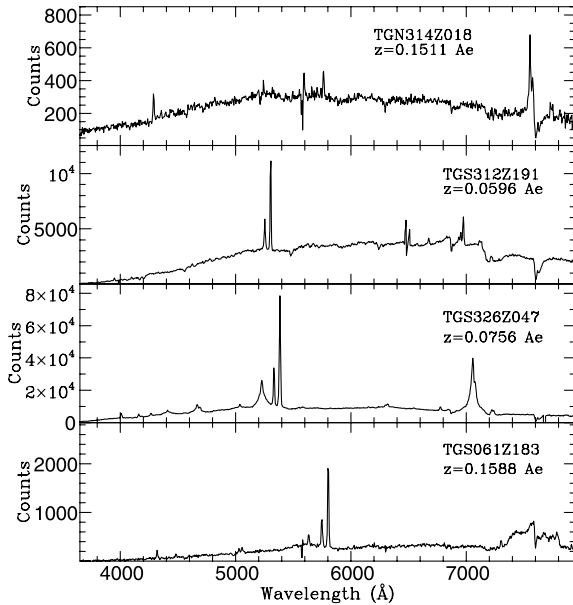


Figure 13. 2dFGRS spectra of four NVSS galaxies detected as X-ray sources in the *ROSAT* All-Sky Survey. All show optical emission lines with line ratios characteristic of active galaxies but, as noted in the text, they are otherwise a diverse class of objects.

which uses a comparably large data set of homogeneous optical spectra.

As can be seen from Fig. 14, the overall agreement between our total (i.e., AGN plus SF) RLF and that of MG is extremely good. This is remarkable, given the differences between the two samples.

(1) Our criteria for determining radio source IDs differ from those used by MC99, as noted in Section 4.6.

(2) All the 2dFGRS redshifts were determined spectroscopically, whereas most of the redshifts listed by MC99 were estimated from optical magnitudes (so that some individual values may have large errors).

Such good agreement between two independent samples chosen in different ways suggests that the RLF is a very robust indicator of the overall density of radio sources in the local Universe.

As can be seen from Fig. 15, however, the agreement between our results and those of MG breaks down when we split our sample into AGN and SF galaxies. We find that the space density of AGN radio sources continues to rise as we go to radio powers as low as $10^{22} \text{ W Hz}^{-1}$, with no sign of a turnover (see Fig. 15). In contrast, MG find a decreasing density of radio AGN below $10^{24} \text{ W Hz}^{-1}$, which is reflected in the divergence of the two AGN LFs in Fig. 15. This turnover in the MG LF for AGN has also been discussed by Brown, Webster & Boyle (2001), who ascribe it to incompleteness in the AGN data used by MG. The good agreement between the faint end of our local RLF for AGN and that derived by Sadler, Jenkins & Kotanyi (1989) for nearby galaxies can be seen in Fig. 18, and strongly supports the view that our values are correct and that the MG sample is incomplete for low-luminosity AGN.

Thus, although we and MG agree on the overall density of radio sources in the local Universe, we disagree on the relative fraction of AGN and SF galaxies below $10^{24} \text{ W Hz}^{-1}$. There are two possible explanations for this, namely a *selection difference* (i.e., the different criteria for inclusion in the two samples select roughly the same *number* of galaxies, but do not necessarily select the same *kind* of galaxies), and a *classification difference*. Our AGN/SF classification is based on optical spectra, whereas MG used the classifications from MC99, which take into account several factors including the radio–optical flux ratio, angular extent of the radio emission, and *IRAS* data where available.

There are 92 galaxies in common between our set of radio source IDs in Table 1 and the LCRS data set used by MC99. Of these, we agree on the classification of 69 (40 AGN, 29 SF), i.e., 75 per cent of the galaxies in common. Of the 25 per cent of galaxies where there is disagreement, most are classified by us as AGN and by MC99 as SF (i.e., for a data set classified by both groups, we find more AGN, and fewer SF galaxies, than MC99).

A detailed comparison of the 2dFGRS and LCRS data sets is outside the scope of this paper, but it seems likely that both

Table 6. Galaxies detected as X-ray sources in the *ROSAT* All-Sky Survey (RASS).

2dFGRS name	<i>ROSAT</i> name	Spectral class	z	Abs. mag.	$\log_{10} P_{1.4}$ (W Hz^{-1})	RSBC count rate (s^{-1})	Notes
TGS312Z191	1RXS J023513.9 – 293616	Ae	0.0596	–22.43	24.58	0.36 ± 0.03	Radio galaxy MRC 0234 – 287
TGN314Z018	1RXS J120226.9 – 012908	Ae	0.1511	–22.01	24.19	0.14 ± 0.03	ULIRG
TGN401Z254	1RXS J133253.5 + 020047	Ae	0.2162	–22.14	26.74	0.25 ± 0.03	Radio galaxy PKS 1330+02
TGS326Z047	1RXS J214636.3 – 305132	Ae	0.0756	–21.48	22.84	0.84 ± 0.07	Seyfert 1
TGS407Z205	1RXS J215809.2 – 312341	Ae	0.0933	–23.01	23.17	0.08 ± 0.02	Seyfert 1
TGS061Z183	1RXS J220924.2 – 245326	Ae	0.1588	–21.51	25.98	0.05 ± 0.02	Radio galaxy PKS 2206 – 251

Table 7. The local radio luminosity function at 1.4 GHz.

$\log_{10} L_{1.4}$ (W Hz ⁻¹)	N	All galaxies $\log_{10} \Phi$ (mag ⁻¹ Mpc ⁻³)	N	AGN $\log_{10} \Phi$ (mag ⁻¹ Mpc ⁻³)	N	Star-forming galaxies $\log_{10} \Phi$ (mag ⁻¹ Mpc ⁻³)
26.6	1	$-7.96^{+0.30}_{-1.0}$	1	$-7.96^{+0.30}_{-1.0}$		
26.2	1	$-8.01^{+0.30}_{-1.0}$	1	$-8.01^{+0.30}_{-1.0}$		
25.8	8	$-6.86^{+0.13}_{-0.19}$	8	$-6.86^{+0.13}_{-0.19}$		
25.4	14	$-6.57^{+0.10}_{-0.14}$	14	$-6.57^{+0.10}_{-0.14}$		
25.0	21	$-6.38^{+0.09}_{-0.11}$	21	$-6.38^{+0.09}_{-0.11}$		
24.6	57	$-5.87^{+0.05}_{-0.06}$	57	$-5.87^{+0.05}_{-0.06}$		
24.2	79	$-5.72^{+0.05}_{-0.05}$	75	$-5.74^{+0.05}_{-0.05}$	4	$-6.98^{+0.18}_{-0.30}$
23.8	110	$-5.46^{+0.04}_{-0.04}$	101	$-5.49^{+0.04}_{-0.05}$	9	$-6.64^{+0.12}_{-0.18}$
23.4	93	$-5.14^{+0.04}_{-0.05}$	66	$-5.32^{+0.05}_{-0.06}$	27	$-5.62^{+0.08}_{-0.09}$
23.0	106	$-4.56^{+0.04}_{-0.04}$	44	$-4.98^{+0.06}_{-0.07}$	62	$-4.77^{+0.05}_{-0.06}$
22.6	80	$-4.14^{+0.05}_{-0.05}$	22	$-4.73^{+0.08}_{-0.10}$	58	$-4.27^{+0.05}_{-0.06}$
22.2	58	$-3.70^{+0.05}_{-0.06}$	8	$-4.52^{+0.13}_{-0.19}$	50	$-3.77^{+0.06}_{-0.07}$
21.8	28	$-3.49^{+0.08}_{-0.09}$	2	$-4.69^{+0.23}_{-0.53}$	26	$-3.52^{+0.08}_{-0.09}$
21.4	4	$-3.59^{+0.18}_{-0.30}$			4	$-3.51^{+0.18}_{-0.30}$
21.0	1	$-3.74^{+0.30}_{-1.00}$			1	$-3.74^{+0.30}_{-1.0}$
20.6	1	$-3.26^{+0.30}_{-1.00}$			1	$-3.26^{+0.30}_{-1.0}$
Total	662		420		242	
$\langle V/V_{\max} \rangle$		0.528 ± 0.011		0.542 ± 0.014		0.503 ± 0.019

selection differences and misclassification of low-power AGN as SF galaxies contribute to the incompleteness of the MG AGN data at low radio powers. The identification criteria used by MC99 may exclude some genuine radio IDs with flux densities above 5 mJy and radio–optical position offsets of less than 10 arcsec (see Section 4.6), and the radio–optical flux ratio which they use in their classification may misclassify some low-power AGN as SF galaxies (especially since the radio sources in low-power AGN are rarely spatially resolved by NVSS, and so cannot be recognized by their radio morphology in the same way as many powerful radio AGN).

8.3 Star-forming galaxies and the local star formation density

As noted earlier, the 2dFGRS excluded most bright, nearby galaxies with $b_J < 14$ mag. To extend our sample to lower radio luminosity, we therefore combined our measured RLF with the local RLF derived by Condon (1989) for galaxies in the Revised Shapley–Ames Catalogue (RSA) (Sandage & Tammann 1981). In doing this, we also increased the values of Φ listed in Table 7 by 5 per cent to correct for the ~ 5 per cent spectroscopic incompleteness of the 2dFGRS (i.e., the spectra in Table 1 with $Q \leq 2$ for which no reliable redshift could be measured). As can be seen from Fig. 16, our results agree well with the Condon RSA values in the small region of overlap. We then fitted an analytic function of the type described by Saunders et al. (1990),

$$\Phi(L) = C \left[\frac{L}{L_{\star}} \right]^{1-\alpha} \exp \left\{ -\frac{1}{2} \left[\frac{\log_{10}(1 + L/L_{\star})}{\sigma} \right]^2 \right\}, \quad (7)$$

to the combined data, and Table 8 summarizes the results.

We can now use the RLF for star-forming galaxies to estimate the local star formation density (i.e., the zero-point of the Madau diagram; Madau et al. 1996). Following Cram (1998) and Haarsma et al. (2000), we assume a Salpeter-like initial mass function

$$\Psi(M) \propto M^{-2.35} \quad (8)$$

over the range 0.1 to 100 M_{\odot} , and convert from a radio luminosity to a star formation rate (SFR) via the relation

$$\text{SFR}(M_{\odot} \text{ yr}^{-1}) = \frac{L_{1.4}(\text{W Hz}^{-1})}{8.85 \times 10^{20}} \quad (9)$$

(Sullivan et al. 2001). The local star formation density at any given

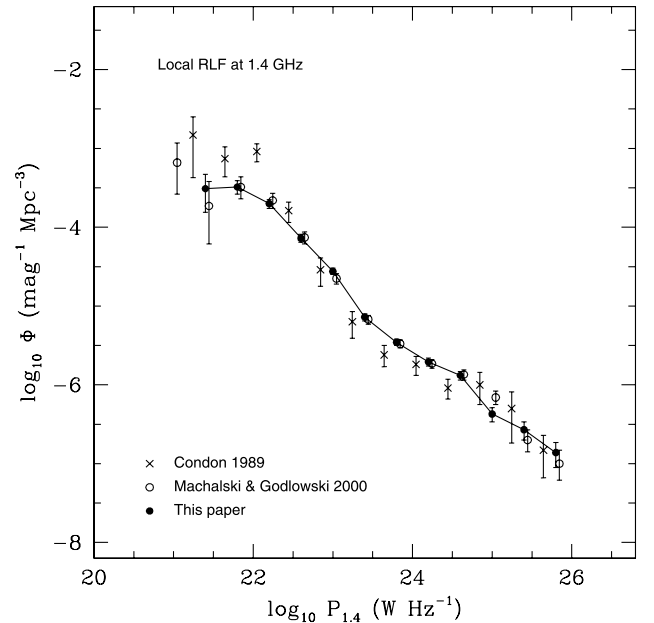


Figure 14. Local RLF derived from the 662 galaxies in Table 1 that are accepted as correct IDs and have radio flux density $S_{1.4} \geq 2.8$ mJy, optical magnitude $14.0 \leq b_J \leq 19.4$ and redshift $0.001 < z < 0.3$. Previous derivations by Condon (1989) and Machalski & Godlowski (2000) are shown for comparison. Between 10^{22} and 10^{24} W Hz⁻¹, our values and those of Machalski & Godlowski are sometimes so close that they are indistinguishable in the diagram.

SFR is then

$$\rho_{\text{SF}} = \text{SFR}(L_{1.4}) \times \Phi(L_{1.4}), \quad (10)$$

where Φ is the local RLF from Tables 7 and 8, multiplied by 1.05 to

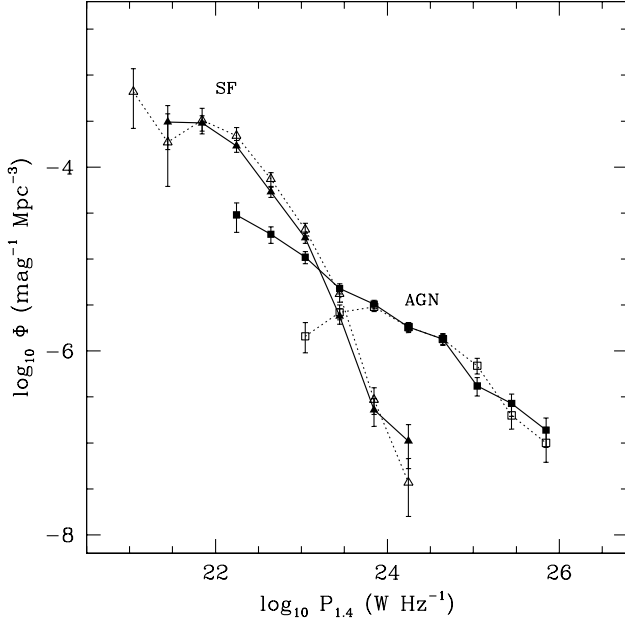


Figure 15. Local RLFs derived for AGN and SF galaxies separately. Filled points connected by solid lines show our own data for AGN (squares) and SF galaxies (triangles). The local RLFs for AGN and SF galaxies derived by Machalski & Godlowski (2000) are plotted using open symbols connected by dotted lines.

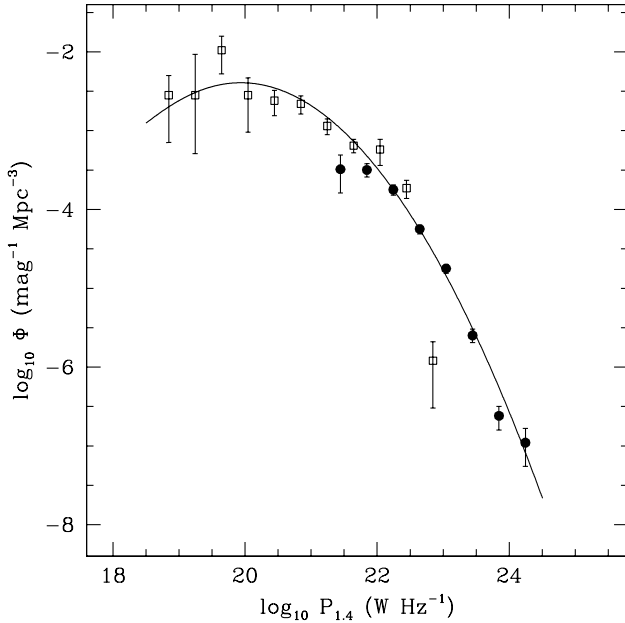


Figure 16. Local RLF for star-forming galaxies, combining data from our sample (filled circles) with values from Condon (1989) for nearby star-forming galaxies from the Revised Shapley–Ames Catalogue (open squares). The NVSS/2dFGRS values of Φ have been increased by 5 per cent to take into account the 95 per cent redshift completeness of the 2dFGRS. The solid line shows the best-fitting analytic function as described in the text.

correct for incompleteness as noted above. Fig. 17 shows the results – our data imply that the greatest contribution to the local star formation density comes from galaxies with SFRs around $10 M_{\odot} \text{ yr}^{-1}$.

As can be seen from Fig. 17, our radio-derived values for the local star formation density are in excellent agreement with the values derived from H α by Gallego et al. (1995, hereafter G95) for galaxies with star formation rates up to $20\text{--}30 M_{\odot} \text{ yr}^{-1}$.

For galaxies with the highest star formation rates ($> 30 M_{\odot} \text{ yr}^{-1}$), however, we find a significantly higher density than G95. The reasons for this are not completely clear – our SF galaxies with high derived SFRs appear to be genuine star-forming galaxies which follow the FIR–radio correlation (see Fig. 10). Where measurements of diagnostic emission-line ratios have been carried out on the 2dF spectra, these also confirm the SF classification (Jackson & Londish 2000).

Our sample volume for galaxies with a high SFR is larger than that surveyed by G95. Their survey covered 471 deg^2 to a depth of $z \leq 0.045$ (beyond which the H α /[N II] lines were shifted out of

Table 8. Parametric fits to the local RLFs for AGN and SF galaxies, using the Saunders et al. (1990) fitting function as described in the text.

Parameter	SF galaxies	AGN	Units
$\log_{10} L_{\star}$	19.55 ± 0.03	24.59 ± 0.03	W Hz^{-1}
α	0.840 ± 0.020	1.58 ± 0.02	
σ	0.940 ± 0.004	1.00 ± 0.13	
$\log_{10} C$	-2.41 ± 0.04	-5.89 ± 0.02	$\text{mag}^{-1} \text{ Mpc}^{-3}$
χ^2	1.86	0.91	

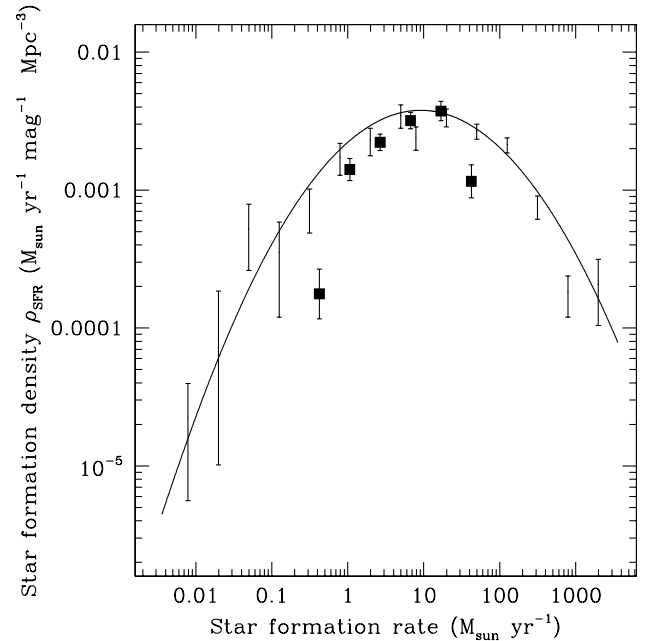


Figure 17. Local star formation density (in $M_{\odot} \text{ yr}^{-1} \text{ mag}^{-1} \text{ Mpc}^{-3}$) for galaxies with star formation rates between 0.01 and $1000 M_{\odot} \text{ yr}^{-1}$. The solid line is derived from the fit to the local RLF for star-forming galaxies (Table 8) after correcting for spectroscopic incompleteness. Error bars from the individual data points used to derive the fit are also shown. Filled squares show the values of local star formation density derived from H α measurements by Gallego et al. (1995).

their passband), i.e., a maximum volume of about $9 \times 10^5 \text{ Mpc}^3$. The equivalent volume for the SF galaxies in our current (325 deg^2) sample is set by the redshift at which the observed radio flux density falls below our 2.8 mJy cut-off. For a galaxy with an SFR of $\sim 100 \text{ M}_\odot \text{ yr}^{-1}$, this redshift is $z \approx 0.084$, giving a volume of $4.5 \times 10^6 \text{ Mpc}^3$, or 5 times the volume surveyed by G95.

Because of this increase in sample volume for stronger radio sources, the 2dFGRS/NVSS SF sample is dominated by galaxies with high star formation rates (well over half the SF galaxies we detect have derived star formation rates above $30 \text{ M}_\odot \text{ yr}^{-1}$, compared to only 5 per cent of the G95 galaxies), so we would expect to have better statistics than G95 for galaxies with high SFRs, assuming that the radio luminosity continues to scale linearly with SFR.

It is possible that at high star formation rates the $\text{H}\alpha$ emission line is increasingly obscured by dust, so that optical surveys underestimate the number of galaxies with very high star formation rates. Deep VLA studies of galaxy clusters at $z \sim 0.4$ (Smail et al. 1999) and local galaxies with ‘post-starburst’ optical spectra (Miller & Owen 2001) suggest that some galaxies may have star-forming regions which are largely hidden by dust. Follow-up observations of the galaxies in Table 1 for which the radio data imply high star formation rates would therefore be valuable.

Integrating under the curve in Fig. 17 gives a local star formation density of $0.022 \pm 0.004 \text{ M}_\odot \text{ yr}^{-1} \text{ Mpc}^{-3}$, which is slightly higher than the value of $0.013^{+0.007}_{-0.005}$ derived by G95 from $\text{H}\alpha$ data. The difference arises mainly because our sample contains more galaxies with high star formation rates ($> 30 \text{ M}_\odot \text{ yr}^{-1}$). For galaxies with star formation rates up to $50 \text{ M}_\odot \text{ yr}^{-1}$, we derive a local density of $0.017 \pm 0.004 \text{ M}_\odot \text{ yr}^{-1} \text{ Mpc}^{-3}$, in excellent agreement with the G95 value.

8.4 Active galaxies and radio galaxies

As in Section 8.3, we combined the NVSS/2dFGRS sample with published data for bright, nearby galaxies to extend our results to lower radio power. Fig. 18 shows the results – the NVSS/2dFGRS data points agree well with the RLF for nearby ($B < 14.0 \text{ mag}$) elliptical and S0 galaxies from Sadler et al. (1989). Once again, we fitted an analytic function as described in Section 8.3, and the results are given in Table 8. However, it is remarkable that the space density of radio-emitting AGN is also well fitted by a single power law of the form

$$\Phi(P_{1.4}) \propto P_{1.4}^{-0.62 \pm 0.03} \quad (11)$$

over almost five decades in luminosity from $10^{20.5}$ to $10^{25} \text{ W Hz}^{-1}$, before turning down above $10^{25} \text{ W Hz}^{-1}$. As pointed out by Sadler et al. (1989), the AGN RLF must also turn down below $10^{20} \text{ W Hz}^{-1}$ in order not to exceed the space density of luminous galaxies.

8.5 Black holes in radio AGN

Franceschini, Vercellone & Fabian (1998) examine the relation between galaxy luminosity, black hole mass and radio power in nearby active galaxies, and conclude that the radio power of an AGN is both a good tracer of supermassive black holes and an estimator of their mass (although Laor 2000 notes that the correlation between radio power and black hole mass shows considerable scatter).

Following the precepts of Franceschini et al. (1998), we can

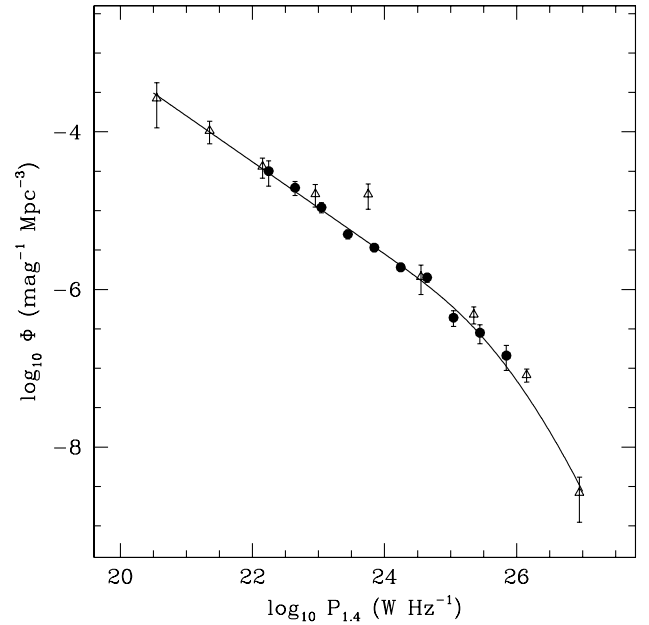


Figure 18. Local RLF for active galaxies, combining data from our sample (filled circles) with values from Sadler et al. (1989) for nearby E/S0 galaxies (open triangles). The Sadler et al. values have been converted to 1.4 GHz , assuming a spectral index of $\alpha = -0.7$. As in Fig. 16, the NVSS/2dFGRS values of Φ have been increased by 5 per cent to take into account the 95 per cent redshift completeness of the 2dFGRS, and the solid line shows the best-fitting analytic function (see Table 8).

estimate the local mass density of black holes from our AGN RLF with the following conversion factors:

$$\log_{10} M_{\text{BH}} (\text{M}_\odot) = 0.376 \log_{10} P_{1.4} (\text{W Hz}^{-1}) + 0.173 \quad (12)$$

and

$$\log_{10} \Phi_{\text{BH}} = \log_{10} \Phi_{1.4} + 0.425. \quad (13)$$

This yields the mass density distribution shown in Fig. 19. In contrast to the star formation density plot shown in Fig. 17, the total mass density of black holes does not converge, but continues to increase down to the lowest values (a few times 10^7 M_\odot) so far probed by radio surveys. Integrating over the values in Fig. 19 gives a total mass density of massive black holes ($M_{\text{BH}} > 7.6 \times 10^7 \text{ M}_\odot$) in galactic nuclei of

$$\rho_{\text{BH}} = 1.8^{+0.4}_{-0.6} \times 10^5 \text{ M}_\odot \text{ Mpc}^{-3}, \quad (14)$$

which is within the range $(1.4 - 2.2) \times 10^5$ derived by Chokshi & Turner (1992) from the optical luminosity function of QSOs. We note that the value derived here is actually a lower limit, since the derived black-hole mass density is still increasing at the lowest values of M_{BH} we can measure. Thus a comparison of black-hole mass densities for radio galaxies in the local Universe and high-redshift QSOs suggests that local radio-emitting AGN are the direct descendants of most or all of the high- z QSOs.

8.6 Redshift evolution of the radio luminosity function

Although the 2dFGRS probes to redshifts of $z \sim 0.3$ to 0.4 where we might expect to see cosmic evolution of the radio source population, only the most luminous objects in our sample can be seen to these distances, and hence we can test for evolutionary

effects only over a narrow range in luminosity. There are already hints that we are seeing evolution in the most powerful AGN in our sample – Table 9 shows the mean values of V/V_{\max} for AGN and star-forming galaxies split into bins in radio luminosity. For AGN with $\log_{10} P_{1.4} > 10^{23} \text{ W Hz}^{-1}$, $\langle V/V_{\max} \rangle$ is significantly higher than the expected value of 0.50, implying that the space density of these objects is higher at higher redshift.

Because the number of objects which we can use to probe evolutionary effects is small, we defer discussion of the RLF evolution to a later paper in this series, which will analyse the full set of 2dFGRS data.

9 DISCUSSION AND CONCLUSIONS

9.1 Main results

We have shown how combining data from large radio continuum and optical redshift surveys allows us to derive accurate local radio luminosity functions (RLFs) for AGN and star-forming (SF) galaxies. Both AGN and star-forming galaxies are significant contributors to the local RLF below $10^{24} \text{ W Hz}^{-1}$ (at higher radio powers, almost all the sources are AGN), so good-quality optical spectra are needed to classify the radio sources correctly.

This paper establishes an accurate local benchmark for future studies of the cosmic evolution of both AGN and star-forming galaxies at higher redshift. The full data set of ~ 4000 radio source spectra, which will become available when the 2dFGRS is completed, should be large enough to measure the evolution of radio galaxies to $z = 0.35$ and the most luminous star-forming galaxies to $z = 0.2$.

9.2 2dFGRS radio-source populations needing further investigation

We showed in Section 6 that there may be a substantial local population of radio-luminous star-forming galaxies (with implied star formation rates of $50 M_{\odot} \text{ yr}^{-1}$ or more) which are not seen in H α emission-line surveys. Determining whether these ‘high-SFR’ galaxies are dust-enshrouded starbursts or misclassified AGN is important if we are to have an accurate census of star formation in the local Universe (if they are indeed starbursts, the ‘high-SFR galaxies’ contribute about 20 per cent of the local star formation density). High-resolution radio imaging, together with infrared spectroscopy, should allow us to determine whether the radio emission seen by NVSS arises mainly from dusty star-forming regions.

Optical spectra of the remaining NVSS/ROSAT sources in the 2dFGRS area (see Section 7) would be valuable in determining whether some radio AGN have been excluded from the 2dFGRS because they have a bright nucleus which leads to them being classified as stars rather than galaxies on sky-survey plates. We estimate that no more than five or six potential members of the current sample have been excluded in this way, but it would be useful to confirm this.

9.3 Prospects for deeper radio and optical observations in the 2dFGRS area

Since the overlap between 2dFGRS galaxies and NVSS radio sources is relatively small – about 5 per cent of NVSS radio sources in the 2dFGRS area are associated with 2dFGRS galaxies, and 1–2 per cent of 2dFGRS galaxies are detected by NVSS – it is

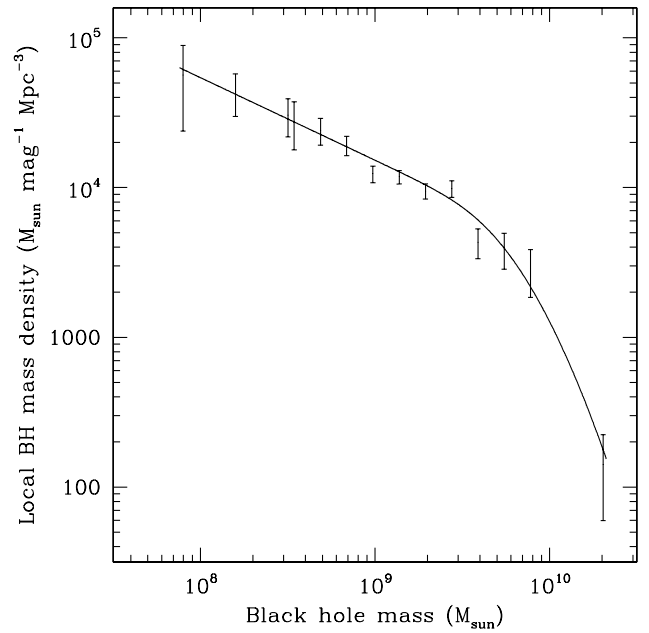


Figure 19. Local mass density (in $M_{\odot} \text{ mag}^{-1} \text{ Mpc}^{-3}$) of black holes, derived from the local radio luminosity function for AGN (Tables 7 and 8), together with the mean relation between radio power and black hole mass from Franceschini et al. (1998). As in Fig. 17, error bars are shown for the individual points used to derive the fit in Table 8.

Table 9. Values of $\langle V/V_{\max} \rangle$ from RLF calculations split into bins in radio power.

$\log_{10} P_{1.4}$ (W Hz^{-1})	— AGN — n	$\langle V/V_{\max} \rangle$	— SF — n	$\langle V/V_{\max} \rangle$
22–23	46	0.50 ± 0.05	141	0.48 ± 0.03
23–24	195	0.55 ± 0.02	65	0.54 ± 0.04
24–25	145	0.55 ± 0.02	4	0.53 ± 0.12

tempting to speculate on what could be achieved with deeper radio and optical observations in the 2dFGRS area.

Radio observations to sub-mJy sensitivities at 1.4 GHz would increase the detection rate for galaxies in the 2dFGRS sample, particularly for star-forming galaxies since many of these lie close to the 2.8-mJy NVSS detection limit (see Section 3.4). For example, observations with a 3σ detection limit of 0.4 mJy at 1.4 GHz could detect galaxies with a star formation rate of $\sim 17 M_{\odot} \text{ yr}^{-1}$ at $z = 0.1$, which is significantly lower than the limit of $\sim 120 M_{\odot} \text{ yr}^{-1}$ at the same redshift for galaxies near the NVSS detection limit of 2.8 mJy.

About 30 per cent of all NVSS radio sources have an optical counterpart visible on the digitized sky survey (i.e., brighter than $b_J \sim 23$ mag). Deep 2dF spectroscopy should be possible to $b_J = 21$ mag (and even fainter for emission-line objects) with integration times of 4–8 h rather than the 40–60 min used by the 2dFGRS, and careful attention to sky-subtraction techniques (Cannon 2001). This would allow spectroscopy of the host galaxies of powerful AGN (and hence studies of their cosmic evolution) to redshifts of $z \sim 0.7$ rather than the $z \sim 0.35$ limit of the 2dFGRS.

9.4 Implications for deep radio surveys to μJy levels

Fig. 20 shows the local RLFs for SF galaxies and AGN over the

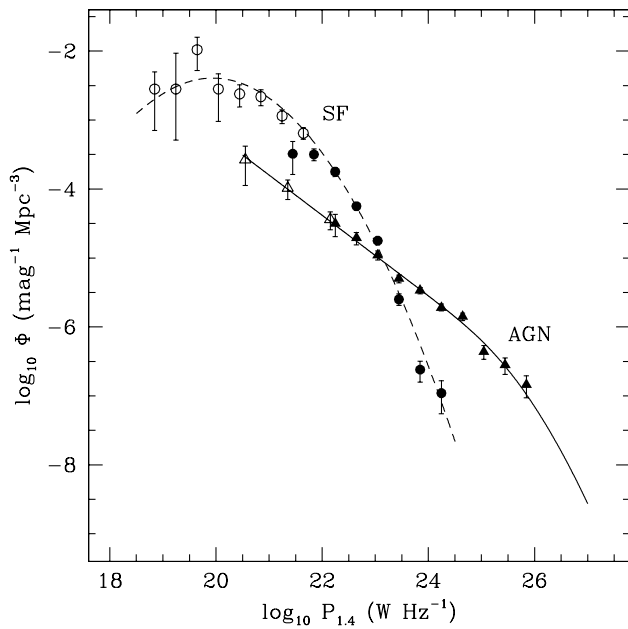


Figure 20. Local radio luminosity functions for AGN and star-forming galaxies, combining 2dFGRS data with nearby RSA spirals (SF) from Condon (1989) and nearby E/S0 galaxies (AGN) from Sadler et al. (1989). Note that both AGN and SF galaxies contribute significantly at all radio powers below $\sim 10^{25} \text{ W Hz}^{-1}$ at 1.4 GHz.

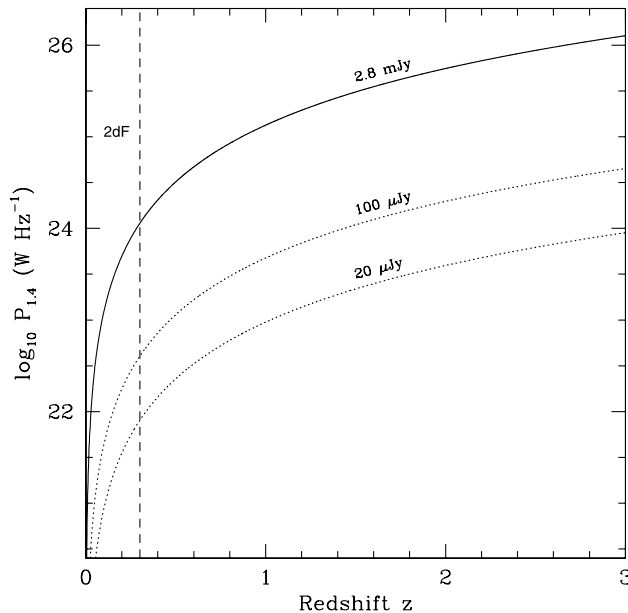


Figure 21. Radio luminosity limits at high redshift for NVSS (2.8-mJy limit) and deeper 1.4GHz surveys (100- and 20- μJy limits). The vertical line at $z = 0.3$ marks the effective redshift limit of the 2dFGRS. Note that at $z \sim 1$, the deepest surveys so far carried out detect galaxies with radio luminosities above about $10^{23} \text{ W Hz}^{-1}$, i.e., in the regime where we expect a mixture of AGN and star-forming galaxies.

whole range in radio power for which data are currently available. The two RLFs cross over (i.e., AGN and SF galaxies contribute equally to the local radio source population) at $P_{1.4} \approx 10^{23.2} \text{ W Hz}^{-1}$. Both AGN and SF galaxies contribute at least 20 per cent of the radio source population over the range $10^{22.5} - 10^{23.7} \text{ W Hz}^{-1}$.

Fig. 21 shows the radio luminosity range probed at different redshifts by 1.4-GHz surveys with flux density limits of 2.8 mJy (NVSS), 100 μJy (e.g. Grappioni et al. 1997; Hopkins et al. 1998) and 20 μJy (e.g. Haarsma et al. 2000). Extrapolating from the local RLF suggests that all μJy -level radio surveys should find a mixture of AGN and SF galaxies at all redshifts, i.e., there is no observational regime in which we can simply assume that a faint radio source arises from a starburst. Deep radio continuum surveys in the Hubble Deep Field (Richards et al. 1998; Garrett et al. 2000) suggest that the μJy radio source population is composed of a mixture of 70–90 per cent spiral and irregular/merging galaxies and 10–30 per cent ellipticals.

A mixture of SF galaxies and AGN is probably present even at flux densities below 1 μJy – Hopkins et al. (2000) remark that in their simulations of the faint radio source population to a flux density limit of 0.1 μJy , the proportion of AGN is still significant. If this is true, then optical/IR spectroscopy will play a key role in disentangling the faint radio source population probed by future deep radio surveys, and partnerships between radio and optical telescopes in mapping out the distant Universe will increase in importance in the years to come.

ACKNOWLEDGMENTS

The 2dF Galaxy Redshift Survey was made possible through the dedicated efforts of the staff of the Anglo-Australian Observatory, both in creating the 2dF instrument and in supporting it on the telescope. This research has made use of the NASA/IPAC Extragalactic Database (NED), which is operated by the Jet Propulsion Laboratory, Caltech, under contract with NASA. We thank Professor Lawrence Cram for helpful conversations about the derivation of star formation rates from radio data, and the referee, Dr I. Snellen, for several perceptive comments which improved the final version of this paper.

REFERENCES

- Allen D. A., Roche P. F., Norris R. F., 1985, *MNRAS*, 213, 67
- Bauer F. E., Condon J. J., Thuan T. X., Broderick J. J., 2000, *ApJS*, 129, 547
- Becker R. H., White R. L., Helfand D. J., 1995, *ApJ*, 450, 559
- Beichman C. A., Neugebauer G., Habing H. J., Clegg P. E., Chester T. J., 1988, *IRAS Catalogs and Atlases Version 2. Explanatory Supplement*
- Bock D. C-J., Large M. I., Sadler E. M., 1999, *AJ*, 117, 1593
- Brown M. J. I., Webster R. L., Boyle B. J., 2001, *AJ*, 121, 2381
- Cannon R., 2001, *AAO Newsletter*, 96, 13
- Chokshi A., Turner E. L., 1992, *MNRAS*, 259, 421
- Clements D. L., Sutherland W. J., Saunders W., Efstathiou G. P., McMahon R. G., Maddox S., Lawrence A., Rowan-Robinson M., 1996, *MNRAS*, 279, 459
- Clements D. L., Saunders W. J., McMahon R. G., 1999, *MNRAS*, 302, 391
- Clowes R. G., Campusano L. E., Leggett S. K., Savage A., 1995, *MNRAS*, 275, 819
- Colless M., 1999, *Phil. Trans. R. Soc. London A*, 357, 105
- Colless M. et al., 2001, *MNRAS*, in press (astro-ph/0106498)
- Condon J. J., 1989, *ApJ*, 338, 13
- Condon J. J., 1992, *ARA&A*, 30, 575
- Condon J. J., Broderick J. J., 1988, *AJ*, 96, 30
- Condon J. J., Kaplan D. L., Yin Q. F., 1997, *AAS*, 191.1402
- Condon J. J., Cotton W. D., Greisen E. W., Yin Q. F., Perley R. A., Taylor G. B., Broderick J. J., 1998, *AJ*, 115, 1693
- Cram L. E., 1998, *ApJ*, 506, 85
- de Grijs M. H. K., Miley G. K., Lub J., de Jong T., 1985, *Nat*, 314, 240
- de Jong T., Klein U., Wielebinski R., Wunderlich E., 1985, *A&A*, 147, L6
- Devereux N. A., Eales S. A., 1989, *ApJ*, 340, 708

- Folkes S. et al., 1999, MNRAS, 308, 459
- Franceschini A., Vercellone S., Fabian A. C., 1998, MNRAS, 297, 817
- Gallego J., Zamorano J., Aragon-Salamanca A., Rego M., 1995, ApJ, 455, L1, (G95)
- Garrett M. A., de Bruyn A. G., Giroletti M., Baan W. A., Schilizzi R. T., 2000, A&A, 361, L41
- Gruppioni C., Zamorani G., de Ruiter H. R., Parma P., Mignoli M., Lari C., 1997, MNRAS, 286, 470
- Haarsma D. B., Partridge R. B., Windhorst R. A., Richards E. A., 2000, ApJ, 544, 641
- Helfand D. J., Schnee S., Becker R. H., White R. L., McMahon R. G., 1999, AJ, 117, 1568
- Helou G., Soifer B. T., Rowan-Robinson M., 1985, ApJ, 298, L7
- Hopkins A. M., Mobasher B., Cram L., Rowan-Robinson M., 1998, MNRAS, 296, 839
- Hopkins A., Windhorst R., Cram L., Ekers R., 2000, Experimental Astronomy, 10, 419
- Ishwara-Chandra C. H., Saikia D. J., 1999, MNRAS, 309, 100
- Jackson C. A., Londish D. M., 2000, Proc. Astron. Soc. Aust., 17, 234
- Jauncey D. L., 1975, ARA&A, 13, 23
- Kapahi V. K., Athreya R. M., van Breughel W., McCarthy P. J., Subrahmanya C. R., 1998, ApJS, 118, 275
- Kim D.-C., Sanders D. B., 1998, ApJS, 119, 41
- Komissarov S. S., Gubanov A. G., 1994, A&A, 285, 27
- Kulkarni S. R. et al., 1998, Nat, 395, 663
- Laor A., 2000, ApJ, 543, L111
- Lawrence A., Walker D., Rowan-Robinson M., Leech K. J., Penston M. V., 1986, MNRAS, 219, 687
- Longair M. S., 1966, MNRAS, 133, 421
- Machalski J., Condon J. J., 1999, ApJS, 123, 41, (MC99)
- Machalski J., Godlowski W., 2000, A&A, 360, 463, (MG)
- Madau P., Ferguson H. C., Dickinson M. E., Giavalisco M., Steidel C. C., Fruchter A., 1996, MNRAS, 283, 1388
- Madgwick D. et al., 2001MNRAS, submitted (astro-ph/0107197)
- Magliocchetti M., Maddox S. J., Lahav O., Wall J. V., 1998, MNRAS, 300, 257
- Miller N. A., Owen F. N., 2001, ApJ, 554, L25
- Moshir M. et al., 1990, IRAS Faint Source Catalogue Version 2.0
- Pence W., 1976, ApJ, 203, 39
- Rengelink R. B., Tang Y., de Bruyn A. G., Miley G. K., Bremer M. N., Röttgering H. J. A., Bremer M. A. R., 1997, A&AS, 124, 259
- Richards E. A., Kellermann K. I., Fomalont E. B., Windhorst R. A., Partridge R. B., 1998, AJ, 116, 1039
- Sadler E. M., Jenkins C. R., Kotanyi C. G., 1989, MNRAS, 240, 591
- Sadler E. M., McIntyre V. J., Jackson C. A., Cannon R. D., 1999, PASA, 16, 247, (Paper I)
- Sandage A., Tammann G. A., 1981, A Revised Shapley-Ames Catalogue of Bright Galaxies. Carnegie Inst., Washington
- Sanders D. B., Mirabel I. F., 1996, ARA&A, 34, 749
- Saunders W., Rowan-Robinson M., Lawrence A., Efstathiou G., Kaiser N., Ellis R. S., Frenk C. S., 1990, MNRAS, 242, 318
- Saunders W. et al., 2000, MNRAS, 317, 55
- Savage A., Wall J. V., 1976, Aust. J. Phys. Astrophys. Suppl., 39, 39
- Schmidt M., 1968, ApJ, 151, 393
- Schoenmakers A. P., Mack K.-H., de Bruyn A. G., Röttgering H. J. A., Klein U., van der Laan H., 2000, A&AS, 146, 322
- Smail I., Morrison G., Gray M. E., Owen F. N., Ivison R. J., Kneib J.-P., Ellis R. S., 1999, ApJ, 525, 609
- Strauss M. A., Huchra J. P., Davis M., Yahil A., Fisher K. B., Tonry J., 1992, ApJS, 83, 29
- Sullivan M. et al., 2001, MNRAS, submitted
- Veilleux S., Kim D.-C., Sanders D. B., 1999, ApJ, 522, 113
- Voges W. et al., 1999, A&A, 349, 389
- Wall J. V., Wright A. E., Bolton J. G., 1976, Aust. J. Phys. Astrophys. Suppl., 39, 1
- Wall J. V., Pearson T. J., Longair M. S., 1980, MNRAS, 193, 683
- Weiler K. W., Montes M. J., Panagia N., Sramek R. A., 1998, ApJ, 500, 51
- White R. L., Becker R. H., 1992, ApJS, 79, 331
- York D. G. et al., 2000, AJ, 120, 1579

This paper has been typeset from a $\text{\TeX}/\text{\LaTeX}$ file prepared by the author.